Biochimica et Biophysica Acta 1837 (2014) 1362–1375

Contents lists available at ScienceDirect

Biochimica et Biophysica Acta

journal homepage: www.elsevier.com/locate/bbabio

Evidence that histidine forms a coordination bond to the A_{0A} and A_{0B} chlorophylls and a second H-bond to the A_{1A} and A_{1B} phylloquinones in $M688H_{PsaA}$ and $M668H_{PsaB}$ variants of *Synechocystis* sp. PCC 6803

Junlei Sun [a,1], Sijie Hao [a,1], Matthew Radle [a], Wu Xu [b], Ivan Shelaev [c], Victor Nadtochenko [c], Vladimir Shuvalov [d], Alexey Semenov [d], Heather Gordon [e], Art van der Est [e,*], John H. Golbeck [a,f,**]

[a] Department of Biochemistry and Molecular Biology, The Pennsylvania State University, University Park, PA 16802, USA
[b] Department of Chemistry, University of Louisiana at Lafayette, Lafayette, LA 70504, USA
[c] Department of Molecular and Chemical Physics, Moscow Institute of Physics and Technology, Dolgoprudny, Moscow Region 141700, Russian Federation
[d] A.N. Belozersky Institute of Physical-Chemical Biology, Moscow State University, Moscow 119991, Russia
[e] Department of Chemistry, Brock University, St. Catharines, ON, Canada L2S 3A1
[f] Department of Chemistry, The Pennsylvania State University, University Park, PA 16802, USA

ARTICLE INFO

Article history:
Received 19 November 2013
Received in revised form 2 April 2014
Accepted 4 April 2014
Available online 16 April 2014

Keywords:
Chlorophyll *a*
Photosynthesis
Photosystem I
A_0
A_1
Phylloquinone

ABSTRACT

The axial ligands of the acceptor chlorophylls, A_{0A} and A_{0B}, in Photosystem I are the Met sulfur atoms of $M688_{PsaA}$ and $M668_{PsaB}$. To determine the role of the Met, His variants were generated in *Synechocystis* sp. PCC 6803. Molecular dynamics simulations on $M688H_{PsaA}$ show that there exist low energy conformations with the His coordinated to A_{0A} and possibly H-bonded to A_{1A}. Transient EPR studies on $M688H_{PsaA}$ indicate a more symmetrical electron spin distribution in the A_{1A} phyllosemiquinone ring consistent with the presence of an H-bond to the C1 carbonyl. Ultrafast optical studies on the variants show that the 150 fs charge separation between P_{700} and A_0 remains unaffected. Studies on the ns timescale show that 57% of the electrons are transferred from A_{0A}^- to A_{1A} in $M688H_{PsaA}$ and 48% from A_{0B}^- to A_{1B} in $M668H_{PsaB}$; the remainder recombine with P_{700}^+ with 1/*e* times of 25 ns and 37 ns, respectively. Those electrons that reach A_{1A} and A_{1B} in the branch carrying the mutation are not transferred to F_X, but recombine with P_{700}^+ with 1/*e* times of ~15 μs and ~5 μs, respectively. Hence, the His is coordinated to A_0 in all populations, but in a second population, the His may be additionally H-bonded to A_1. Electron transfer from A_0 to A_1 occurs only in the latter, but the higher redox potentials of A_0 and A_1 as a result of the stronger coordination bond to A_0 and the proposed second H-bond to A_1 preclude electron transfer to the Fe/S clusters.

1. Introduction

Photosynthetic reaction centers (RCs) exist in two varieties depending on the identity of the terminal electron acceptor. Type II RCs, which include the purple bacterial RC and Photosystem II (PS II), incorporate a mobile quinone as the terminal acceptor. In contrast, in type I RCs, which include the homodimeric RCs in *Chlorobium*, *Heliobacteriaceae* and *Chloracidobacterium* and the heterodimeric RC, Photosystem I (PS I), in plants and cyanobacteria, the terminal acceptor is a bound iron-sulfur (FeS) cluster [1]. Cyanobacterial PS I is composed of 12 polypeptides, 96 chlorophylls (Chl), 22 carotenoids, three [4Fe-4S] clusters, two phylloquinones (PhQ), and four lipids. The membrane-spanning polypeptides, PsaA and PsaB, form a near C_2-symmetric heterodimeric core that incorporates the majority of the cofactors [2] (Fig. 1). The electron transfer chain begins at a special pair of Chl *a*/*a*′ molecules [3] (Chl *a*′ is the C-10 epimer of Chl *a*) termed P_{700}, after which it diverges into A- and B-branches. The branches contain a Chl *a* in the intermediate A_{accA} and A_{accB} sites, as well as in the acceptor A_{0A} and A_{0B} sites, and a phylloquinone in the A_{1A} and A_{1B} sites. The A- and B- branches converge at the interpolypeptide [4Fe-4S] cluster, F_X, which bridges the PsaA and PsaB heterodimer. A third polypeptide, PsaC, is located on the stromal side of PS I, and contains two additional [4Fe-4S] clusters named F_A and F_B (reviewed in Ref. [4]).

It was recently shown that upon preferential excitation of P_{700} the formation of the $P_{700}^+A_0^-$ charge-separated state is complete within 100 fs [5]. The lifetime of the $P_{700}^+A_{0A}^-$ or $P_{700}^+A_{0B}^-$ radical pair is short, and within 13 to 26 ps the electron is passed to A_{1A} or A_{1B} [5,6]. Forward electron transfer from A_{1A}^- or A_{1B}^- to F_X occurs with lifetimes of ~200 ns and ~20 ns, respectively [7–9]. The electron is passed serially through the F_X, F_A and F_B clusters, after which it is donated to soluble ferredoxin

Abbreviations: PS I, Photosystem I; Chl, chlorophyll; RC, reaction center; PhQ, phylloquinone; flv, flavodoxin; DCPIP, 2,6-dichlorophenolindophenol; EPR, electron paramagnetic resonance

* Corresponding author. Tel.: +1 905 688 5550.
** Correspondence to: J.H. Golbeck, Department of Biochemistry and Molecular Biology, The Pennsylvania State University, University Park, PA 16802, USA. Tel.: +1 814 865 1163.
E-mail addresses: avde@brocku.ca (A. van der Est), jhg5@psu.edu (J.H. Golbeck).

[1] Junlei Sun and Sijie Hao should be considered co-first authors.

http://dx.doi.org/10.1016/j.bbabio.2014.04.004
0005-2728/

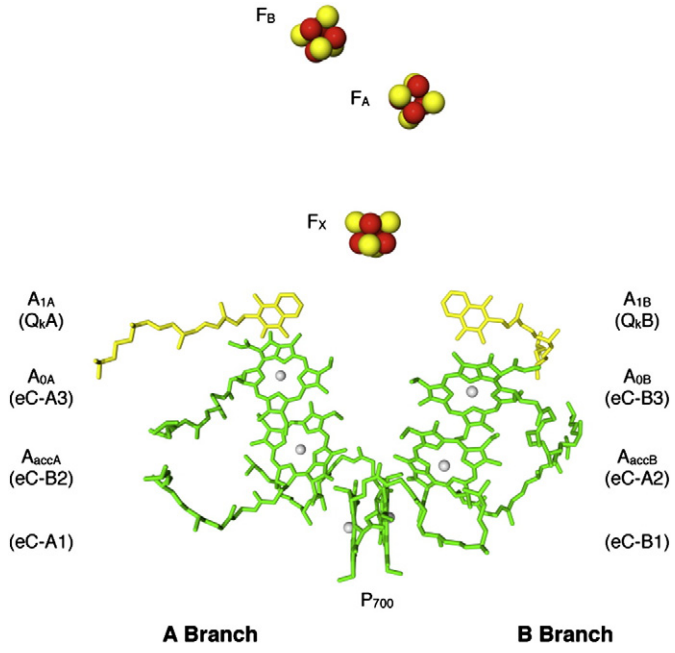

Fig. 1. The organization of the electron transfer cofactors in cyanobacterial Photosystem I. The figure has been constructed using the atomic coordinates in PDB ID: 1JB0 [2]. The names refer to the nomenclature in the spectroscopic literature; the names in parenthesis refer to the nomenclature in the crystallographic database.

or flavodoxin. P_{700}^{+} in turn is reduced by plastocyanin or soluble cytochrome c_6, at which point all bound cofactors have returned to their ground states. When no soluble electron acceptors or donors are present, the charge separated state between P_{700}^{+} and $[F_A/F_B]^{-}$ recombines within ~50 ms [10,11].

The most unusual feature of the acceptor Chls in the A_{0A} and A_{0B} sites is that the central Mg^{2+} is axially ligated to the sulfur atoms of $M688_{PsaA}$ and $M668_{PsaB}$ [2]. Based on the concept of Lewis acids and bases, it is typical to have strong interactions between ligands and metal centers as hard acids and hard bases. The central Mg^{2+} ion of the Chl *a* molecule is a relatively hard acid while oxygen and nitrogen atoms are hard bases. This partially explains the overwhelming preference of Chl *a* for nitrogen and oxygen atoms in both PS I and PS II. In contrast, sulfur has a relatively large radius and a high polarizability, and is a soft Lewis base. Therefore, the interaction between the S atom of the Met side chain and the Mg^{2+} ion of Chl *a* is expected to be weak. Nonetheless, the Met ligand to the Chls in the A_{0A} and A_{0B} sites is conserved in PS I from all known species probably because it is instrumental in achieving the low reduction potential required of this acceptor. Accordingly, a change in the identity of the axial ligand from a Met to a His could be expected to raise its reduction potential, and hence alter the kinetics of electron transfer from A_{0A} to A_{1A} and from A_{0B} to A_{1B}.

A number of studies have already been carried out on *Chlamydomonas reinhardtii* [12–17] and *Synechocystis* sp. PCC 6803 [18–22] in which the methionines that coordinate to A_{0A} and A_{0B} have been altered. In *C. reinhardtii* these residues are $M684_{PsaA}$ and $M663_{PsaB}$ and in *Synechocystis* sp. PCC 6803 they are $M684_{PsaA}$ and $M659_{PsaB}$. Here, we will use the residue numbering for *Thermosynechococcus elongatus* $M688_{PsaA}$ and $M668_{PsaB}$ throughout for both organisms to facilitate comparison with the X-ray crystal structure. Different variants have been generated, and different techniques have been employed, in the study of the variant PS I in these two organisms. In *C. reinhardtii*, $M688_{PsaA}$ and $M668_{PsaB}$ have been replaced with Leu, Ser and His [12–17], and in *Synechocystis* sp. PCC 6803 with Leu, Asn and His [18–22]. In *C. reinhardtii* the His variants have been studied the most extensively. In an ultrafast optical study in the red, long-lived difference spectra observed in the $M688H_{PsaA}$ and $M668H_{PsaB}$ variants were assigned to $(A_{0A}^{-}–A_{0A})$ and $(A_{0B}^{-}–A_{0B})$, respectively and were interpreted to indicate that forward electron transfer beyond A_0 was either blocked or slowed in the branch carrying the mutation [13]. The amplitudes of the $(A_{0A}^{-}–A_{0A})$ and $(A_{0B}^{-}–A_{0B})$ difference spectra were nearly identical in the two variants, suggesting roughly equal use of both branches. A subsequent study at 390 nm showed that formation of phyllosemiquinone in both variants decreased to about one-half of that in the wild type, a result implying that electron transfer is blocked between A_0 and A_1 in the affected branch [16]. An EPR study of the $M688H_{PsaA}$ variant at 265 K showed the absence of an electron spin polarized (ESP) signal, suggesting that the $P_{700}^{+}A_{1A}^{-}$ radical pair cannot be formed and that B-branch transfer, if present, does not produce an ESP signal [12]. In a more recent study in deuterated whole cells of the $M688H_{PsaA}$ variant, a spin-polarized spectrum was detected at 100 K and assigned to the radical pair $P_{700}^{+}A_{1B}^{-}$ [17]. Pulse EPR studies revealed that in the presence of reduced F_X, the decay of the out-of-phase spin polarized signal in the wild type was biphasic but that it was monophasic in the $M688H_{PsaA}$ and $M668H_{PsaB}$ variants, with lifetimes of ~3 μs and ~17 μs, respectively [12,14]. The echo modulation frequencies were different in the two variants and were explained as a result of the difference in the spin-spin coupling in $P_{700}^{+}A_{1A}^{-}$ and $P_{700}^{+}A_{1B}^{-}$. The wild type echo decays and modulation curves could be reconstructed as a linear combination of the signals of the two radical pairs. These data are consistent with a blockage of electron transfer from A_0^{-} to A_1 in Met to His variants of *C. reinhardtii*.

In *Synechocystis* sp. PCC 6803, the Leu and Asn variants have been the most extensively studied. Ultrafast optical investigations of the A-side variants, $M688L_{PsaA}$ and $M688N_{PsaA}$, indicated that even though forward electron transfer from A_0^{-} was slowed by a factor of 3 to 10 [19], the $P_{700}^{+}A_{1A}^{-}$ radical pair was nevertheless formed [18]. In the B-side variants, $M668L_{PsaB}$ and $M668N_{PsaB}$, the kinetics of forward electron transfer from A_0^{-} were relatively unaffected. A transient EPR study of the $M688L_{PsaA}$ variant indicated a change in the polarization patterns of both $P_{700}^{+}A_{1A}^{-}$ and $P_{700}^{+}F_X^{-}$. These changes were attributed to an increased lifetime of A_0^{-}, which allows a greater degree of singlet-triplet mixing during the lifetime of the $P_{700}^{+}A_{0A}^{-}$ radical pair. The increased lifetime of A_0^{-} also led to an increased amount of the triplet state of P_{700}, which is formed as a result of $P_{700}^{+}A_{0A}^{-}$ recombination [18]. A 95 GHz (W-band) time-resolved EPR study of the $M688N_{PsaA}$ and $M668N_{PsaB}$ variants showed that at 100 K, the EPR observables of the $M668N_{PsaB}$ variant were similar to those of the wild type, while the data from the $M688N_{PsaA}$ variant were distinctly different [20]. An analysis of the out-of-phase echo modulations in the wild type and $M668N_{PsaB}$ variant gave a single population of radical pairs assigned to $P_{700}^{+}A_{1A}^{-}$, while in the $M688N_{PsaA}$ variant gave two populations assigned to $P_{700}^{+}A_{1A}^{-}$ and $P_{700}^{+}A_{1B}^{-}$ in a ratio of 0.7:0.3. A time-resolved EPR study of the same variants at X-band showed that at 295 K, the lifetime of electron transfer from A_1^{-} to F_X in the $M688N_{PsaA}$ variant was shorter (160 ns) than in the wild type and the $M668N_{PsaB}$ variant (260 ns) [21]. The fits to the data indicated that the fraction of A_{1A}^{-} to F_X electron transfer was ~95% in the $M668N_{PsaB}$ variant, ~60% in the $M688N_{PsaA}$ variant, and ~85% in the wild type. Thus, the data are consistent with electron transfer *past* A_0 to A_1 in the Met to Leu and Asn variants of *Synechocystis* sp. PCC 6803. A recent low temperature EPR study performed on Met to His variants of *Synechocystis* sp. PCC 6803 [22] indicates that the situation may be more complicated. Whereas the decay of the electron spin echo from the $P_{700}^{+}A_1^{-}$ radical pair is biphasic at 100 K in wild-type PS I, in the presence of reduced F_X only the 20 μs kinetic phase was present in the $M668H_{PsaB}$ variant and only the 3 μs kinetic phase was present in the $M688H_{PsaA}$ variant. Hence, in agreement with the studies performed on Met to His variants in *C. reinhardtii*, electron transfer from A_0 to A_1 appeared to be blocked in Met to His variants of *Synechocystis* sp. PCC 6803.

Given this discrepancy, as well as the relative lack of information on electron transfer beyond A_{1A} and A_{1B} in the His variant in *Synechocystis* sp. PCC 6803, we decided that a more thorough study was warranted. We were particularly motivated by the location of the Met residues,

which are positioned midway between A_0 and A_1. When judged visually, the His imidazole nitrogens appear able to provide a ligand to either or both cofactors. Thus, it is possible that the substitution of His for Met could influence the properties of either or both A_0 and A_1. Here we report time-resolved EPR and optical data on electron transfer through A_0 and A_1 in M688N_{PsaA} and M668N_{PsaB} variants of *Synechocystis* sp. PCC 6803. Most of the studies were carried out at room temperature without prior reduction of F_A, F_B and F_X in order to avoid the possibility that electron transfer at low temperature may differ from that at room temperature as well as the possibility that the pathway may be influenced by the presence of reduced F_A, F_B and F_X. A comparison of the M668H_{PsaB} and M668H_{PsaB} variants in *C. reinhardtii* and *Synechocystis* sp. PCC 6803 and a discussion the temperature dependence of the electron transfer will be presented in a forthcoming paper.

2. Materials and methods

2.1. Molecular dynamics simulations

The details of the molecular dynamics simulations are described in the supporting information. Briefly, the M688H_{PsaA} point mutation was introduced into the X-ray structure of *T. elongatus* PS I [2] using PyMOL with the His residue mono-protonated on the δ-nitrogen (Fig. 2). The structural model was heated from 0 K to 300 K allowing all atoms to move and then heated further to 500 K with the backbone atoms of the protein fixed but with all amino acid side chains, ions, water and cofactors unconstrained. The model was then equilibrated at 500 K and 100 conformers of the equilibrated system were chosen at random. These conformers were each energy-optimized and then analyzed to give histograms of interatomic distances.

2.2. Generation of the point mutants and isolation of PS I complexes

The point mutants M688H_{PsaA} and M668H_{PsaB} were generated as described [23]. The QuickChange site directed mutagenesis kit (Stratagene Inc.) was used to introduce the desired point mutations into the pIBC and pBC+ plasmids. The mutated pIBC plasmid was used to transform the pWX3 recipient strain to generate the M688H_{PsaA} variant, and the mutated pBC+ plasmid was used to transform the pCRTΔB recipient strain to generate the M668H_{PsaB} variant. Transformants were selected and segregated under low light intensities with increasing chloramphenicol concentration from 5 μg/mL to 50 μg/mL. DNA fragments containing the mutation sites were amplified by PCR from genomic DNA of the variant cells and were sequenced to confirm full segregation and the desired nucleotide change. Preparation of thylakoid membranes and isolation of PS I trimers were performed using a nonionic detergent *n*-dodecyl-β-D-maltoside according to previously published procedures [24].

2.3. Physiological and biochemical characterization

The *Synechocystis* sp. PCC 6803 wild type and variant strains were cultured in β-HEPES medium (with 10 μg/mL chloramphenicol for the variants) bubbled with 3% CO_2 in a 30 °C water bath illuminated by fluorescence light tubes at different intensities. Growth rates of the liquid cultures were monitored by the absorbance at 730 nm using a Cary-14 spectrophotometer (Bogart, GA) as described in Ref. [24]. Cultures grown to 0.5 OD_{730nm} under low light were harvested by centrifugation. The content of Chl and carotenoids were determined according to Refs. [25–27]. The 77 K fluorescence emission spectra were measured as described in Ref. [28]. The electron throughput of PS I was measured by the rates of light-driven flavodoxin reduction as described in Ref. [29]. PS I complexes were suspended at 5 μg Chl/mL

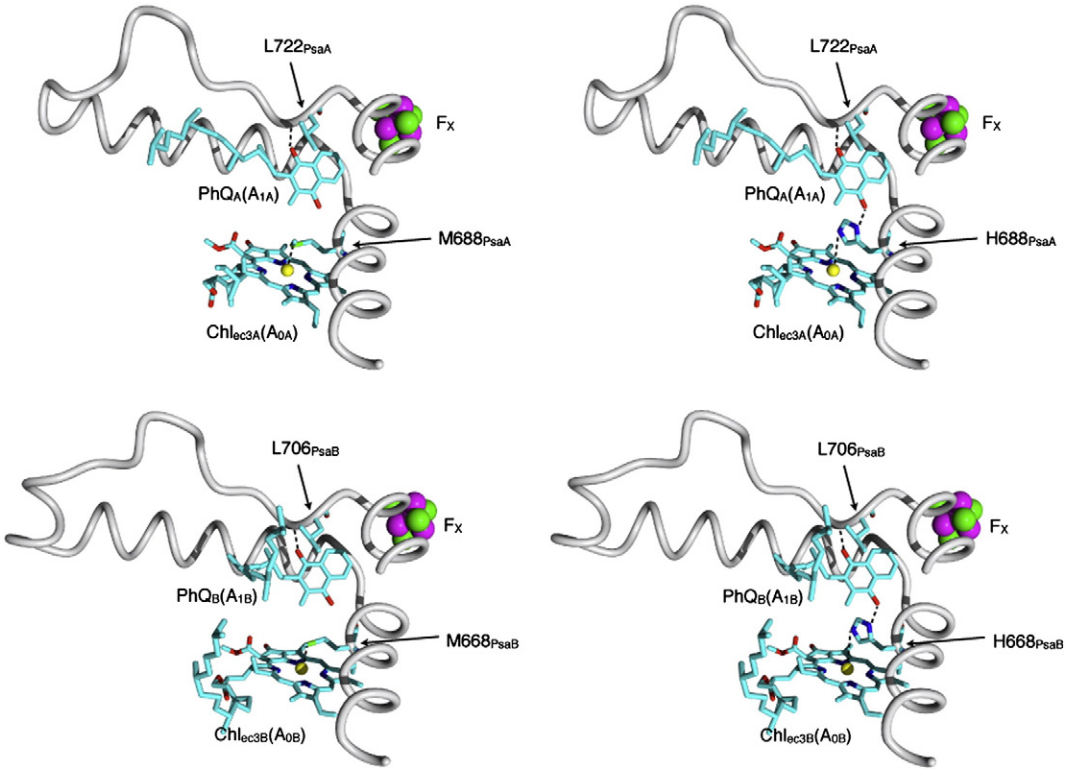

Fig. 2. The A_{1A} and A_{1B} binding sites in both branches of PS I and the tentative conformation of the M688H_{PsaA} and M668H_{PsaB} variants. Only a small portion of the secondary structure and important residues are shown. The amino acid residues and cofactors are colored coded. Tentative hydrogen bonds are denoted as dashed lines.

in 50 mM Tris/HCl, pH 8.3, containing 50 mM Mg_2Cl, 6 μM phenazine methosulfate (PMS), 15 μM flavodoxin, 6 mM sodium ascorbate and 0.05% *n*-dodecyl-β-D-maltoside. The absorbance change at 467 nm was monitored using a commercial LED pump-probe spectrometer JTS-10 (Bio-Logic, France). Actinic illumination was provided by a high-power red LED (680 ± 50 nm); probe pulses were generated by a high-power white LED filtered through a 467 nm interference filter (Edmund Optics, Inc.). The phylloquinone content of PS I trimers from the wild-type, $M688H_{PsaA}$ and $M668H_{PsaB}$ variants was measured according to the protocol described in Ref. [24].

2.4. Electron paramagnetic resonance spectroscopy

Room temperature X-band transient EPR experiments were carried out using a modified Bruker E200 series bridge equipped with a rectangular resonator and a flat cell. The loaded Q-value for the resonator was about $Q = 3000$, equivalent to a rise time $\tau_r = Q/(2\pi \times \nu_{mw}) \approx 50$ ns. The samples were illuminated at 532 nm using the second harmonic of a Q-switched Continuum Surelite Nd:YAG laser operating at 5 Hz. Low temperature X-band transient EPR experiments were carried out using a modified Bruker ESP-300E series bridge equipped with a Bruker model 4118 dielectric ring resonator and a Bruker model ER4118CF low temperature cryostat. The Chl concentration of all samples was 1 to 2 mg Chl/ml and sodium L-ascorbate and PMS were added to final concentrations of 50 mM and 5 μM, respectively.

2.5. Time-resolved optical spectroscopy on the ns to s timescale

Flash-induced absorbance changes at room temperature were measured at 480 nm and 820 nm using laboratory-built spectrophotometers, which are described in detail in the supporting information. The PS I samples were at a concentration of 100 μg Chl mL^{-1} in 50 mM Tris/HCl buffer at pH 8.3 and contained 5 mM sodium L-ascorbate, 10 μM 2,6-dichlorophenolindophenol (DCPIP), 0.05% *n*-dodecyl-β-D-maltoside. Measurements at 480 nm were made on a timescale from 2 ns to 200 μs in a 1 cm × 1 cm quartz cuvette. At a delay time of ~200 μs, the actinic effect of the 480 nm light decreased the amount of photooxidizable P_{700} by 5%, hence measurements at 480 nm were terminated at 200 μs. Measurements at 820 nm were made on a timescale from 2 ns to 2 s in a cuvette with a path length of 1 cm, and a width of 0.4 cm. For both detection wavelengths, the sample was excited by a frequency-doubled (λ = 532 nm), Q-switched Nd:YAG laser (DCR-11; Spectra Physics, Mountain View, CA) operated in the short pulse mode (~3 ns). The time between flashes was 3 s for measurements at 480 nm and 820 nm. The output was measured to be 30 mJ/pulse, and was attenuated to 5% by neutral density filters (Edmund Optics, Barrington, NJ).

The data were analyzed by fitting with a multi-exponential function plus a constant using the Marquardt least-squares algorithm programed in Igor Pro v.6.3 (Wavemetrics, Portland, OR).

2.6. Time-resolved optical spectroscopy on the fs and ns timescale

Transient absorption spectra were measured at sub-ns timescales using a femtosecond pump-supercontinuum probe setup. The output of a Ti:sapphire oscillator (800 nm, 80 MHz, 40 fs, Tsunami, Spectra-Physics) was amplified by a regenerative amplifier system (Spitfire, Spectra-Physics) up to 1 mJ/pulse at a repetition rate of 1 kHz. The amplified pulses were split into two beams. One half of the energy was directed to a non-collinearly phase-matched optical parametric amplifier. The output, which was centered at 720 nm with a bandwidth of 40 nm (fwhm), was subsequently compressed by a pair of quartz prisms. The resulting Gaussian-shaped pulse had a width of 20 fs and was used as the pump pulse. The other half of the energy was focused into a quartz cell with H_2O to generate supercontinuum probe pulses. The pump and probe pulses were time delayed with respect to each other by means of a computer-controlled delay stage. They were attenuated, recombined, and focused into the sample cell with an optical length to the spot of 100 μm. The pump pulse had a diameter of 300 μm, and was attenuated to an energy of 20 nJ at a repetition rate of 15 Hz. The relative polarizations of pump and probe beams were adjusted to 54.7° (magic angle), alternatively the polarization of pump and probe beams was parallel and perpendicular. In the latter case, the polarization of the probe signal could be detected. After exiting the sample, the supercontinuum was dispersed by a polychromator (Acton SP-300) and detected using a CCD camera (Roper Scientific SPEC-10). Absorption difference spectra $\mathbf{\Delta A}(t, \lambda)$, where **ΔA** is the change in optical absorbance, were recorded over a range of 400 nm to 740 nm. The measured spectra were corrected for group delay dispersion of the supercontinuum using a procedure described previously [30]. The experimental data were analyzed using laboratory-written software for MatLab®. Experiments were carried out at 6 °C in a 0.2 mm path length flow optical cell with optical windows of 0.1 mm thickness. The circulation rate in the flow cell was sufficiently fast to avoid multiple excitation of the same sample volume.

3. Results

3.1. Molecular dynamics simulations of the $M688H_{PsaA}$ variant

Fig. 2 depicts the region surrounding the A_0, A_1, and F_X cofactors in wild type PS I in the 2.5 Å resolution X-ray crystal structure of *T. elongatus* (1JB0) [2]. The structures of the $M688H_{PsaA}$ and $M668H_{PsaB}$ variants were generated using PyMOL without any energy minimization. On the PsaA-side (left) and PsaB-side (right), the sulfur atoms of $M688_{PsaA}$ and $M668_{PsaB}$ are at a favorable distance to act as (weak) ligands to the Mg^{2+} of the A_{0A} and A_{0B} Chls, respectively. The backbone nitrogens of $L722_{PsaA}$ and $L706_{PsaB}$ participate in H-bonds to the corresponding C4 carbonyl groups of the A_{1A} and A_{1B} phylloquinones. When Met is replaced by His and no other changes are made to the structure of the protein backbone, the ε-nitrogen of the imidazole ring appears to be positioned so that it can act as a ligand to the Mg^{2+} of Chl in the A_0 sites while the δ-nitrogen is located in a favorable position for H-bonding to the C1 carbonyl group of phylloquinone in the A_1 sites.

Based on these initial observations, we turned to modeling to explore possible structures for the $M688H_{PsaA}$ variant. The simulations produce families of conformers that correspond to local energy minima. The protonation state of the imidazole ring is unknown. However, since hydrogen bonding to the C1 carbonyl oxygen requires protonation of the δ-nitrogen and coordination to Mg^{2+} requires deprotonation of the ε-nitrogen, we used a starting model with $H688_{PsaA}$ monoprotonated on the δ-nitrogen. The tautomeric form with the ε-nitrogen protonated and the δ-nitrogen deprotonated was not considered. The distribution of calculated distances from the $H688_{PsaA}$ ε-nitrogen to the Mg^{2+} ion of the Chl *a* molecule are summarized in Fig. 3**A**. The distribution is very narrow with the most probable distance being 2.3 Å. The sum of the covalent radii of Mg^{2+} and N is 2.12 Å. Hence, the ε-nitrogen of $His688_{PsaA}$ can be considered to be coordinated to the A_{0A} Chl in all of the calculated conformers.

The distance from the δ-nitrogen of $H688_{PsaA}$ to the C1 carbonyl oxygen is displayed in Fig. 3**B**. In this case, a broader distribution is found. The most likely distance is 3.4 Å; the range of the distances is between 3.0 Å and 3.9 Å. If the cut-off distance of a hydrogen bond is set to 2.8 ± 0.3 Å (10%), a hydrogen bond from the δ-nitrogen to the C1 carbonyl oxygen of the phylloquinone is found in 6 out of the 100 conformers. The C4 carbonyl oxygen of the PhQ forms a hydrogen bond to the backbone nitrogen of $Leu722_{PsaA}$ (Fig. 2). The distance of this hydrogen bond is 2.7 Å in wild type PS I. The distance from the backbone N of $L722_{PsaA}$ to the C4 carbonyl oxygen in the $M688H_{PsaA}$ variant is presented in Fig. 3**C**. The most likely distance is 3.1 Å; the range of the distances is between 2.9 Å and 3.3 Å. The distance from the majority of the 100 conformers fall in the range of 2.8 ± 0.3 Å, thereby qualifying

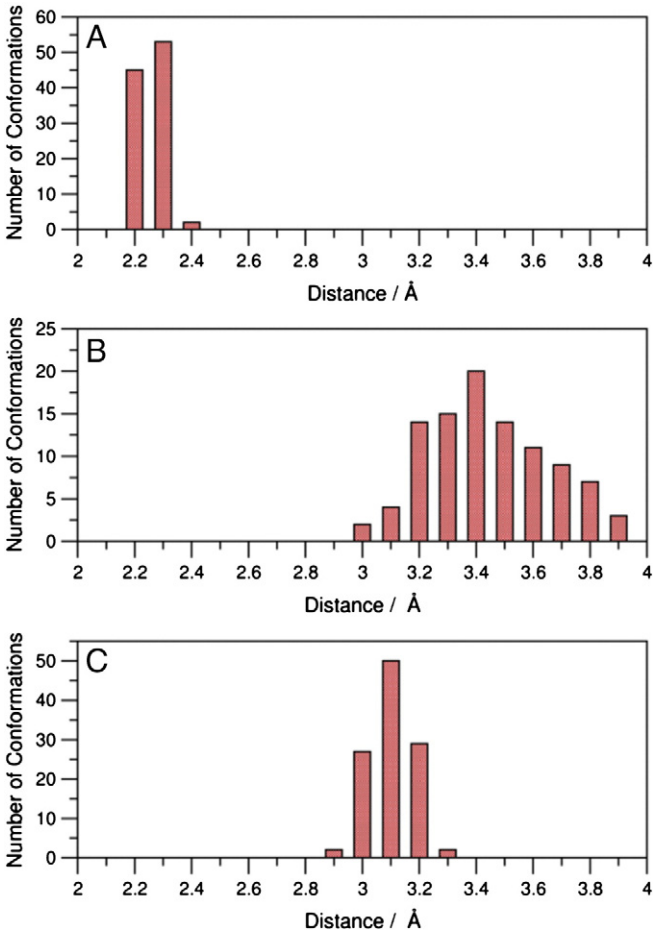

Fig. 3. Predicted protein–cofactor interaction distances for A_{1A} and A_{0A} in the $M688H_{PsaA}$ variant. The bars in the histograms show the number of conformers in which a given distance is obtained from the molecular dynamics simulations. Distances are plotted on the same scale for easy comparison. **A**. Distance from the ε-nitrogen of $His688_{PsaA}$ to the Mg^{2+} of A_0 Chl. **B**. Distance from the δ-nitrogen of $His688_{PsaA}$ to the C1 carbonyl oxygen of the A_{1A} PhQ. **C**. Distance from the backbone nitrogen of $Leu722_{PsaA}$ to the C4 carbonyl oxygen of the A_{1A} PhQ.

as a hydrogen bond according to the distance criterion. The fact that this H-bond is retained in the calculations serves to validate the molecular dynamics simulation procedure.

Together, the histograms in Fig. 3 indicate that in the calculated conformers, the His coordinates to the A_0 chlorophyll and in most cases phylloquinone remains H-bonded to $L722_{PsaA}$. H-bonding between A_1 and the δ-nitrogen of $H688_{PsaA}$ is seen in some of the conformers but there is a relatively wide distribution of possible distances. Here it is important to emphasize that the conformational space that is accessible in the folded protein is highly restricted compared to the conformational space sampled in the molecular dynamics simulations. Thus, the simulations only predict possible low energy conformations but not into which of these conformers the protein folds. Nonetheless, the presence of a fairly broad distribution of distances between the δ-nitrogen of $H688_{PsaA}$ and the C1 carbonyl oxygen of the phylloquinone is an indication that the mutation may cause disorder in the structure.

3.2. Physiological characterization of the wild type and the variant strains

The $M688H_{PsaA}$ and $M668H_{PsaB}$ variants were constructed in *Synechocystis* sp. PCC 6803 to verify the predictions of the molecular dynamics simulations, *i.e.* whether His is coordinated to the A_0 Chl and whether there is an H-bond from the His to the C1 carbonyl group of the A_1 phylloquinone. The physiological properties of the two variants were studied first. The doubling time of the wild type and variant strains were compared at two light intensities under photoautotrophic growth conditions (Fig. 4**A**). Under a low-light regime of 50 μE m^{-2} s^{-1}, both the wild type and the $M668H_{PsaB}$ variant grew with a doubling time of 12 hr, while the $M688H_{PsaA}$ variant grew slower, with a doubling time of 15 hr. Under a high light regime of 200 μE m^{-2} s^{-1}, the growth rates of the wild type and $M668H_{PsaB}$ variant began to diverge, showing doubling times of 8 and 9 hr, respectively, while the $M688H_{PsaA}$ variant was light-sensitive and failed to grow.

The decreased growth rates of the cyanobacterial variants could be a consequence of an altered pigment content, a lower PS I/PS II ratio, or a decrease in the efficiency of electron transfer through PS I. The amount of Chl and carotenoid was determined on a per cell basis in *Synechocystis* sp. PCC 6803 cells grown to early log phase under a low light regime (Fig. 4**B**). Although small variations were detected, the $M688H_{PsaA}$ and $M668H_{PsaB}$ variant strains contained approximately the same amount of Chl and carotenoids as the wild type. The PS I/PS II ratio was estimated by measuring the low-temperature (77 K) fluorescence emission of whole cells when excited at 440 nm. PS II and its accessory pigments show emission maxima at 685 and 695 nm, and PS I shows a emission maximum at 721 nm [31]. The emission spectra of the wild type and the variants were normalized to the PS II peaks at 695 nm, and the amplitudes at 721 nm were compared to approximate the relative amount of PS I. Both variant strains (Fig. 4**C**) showed a lower PS I/PS II ratio than to the wild type, but the decline was more pronounced in the $M688H_{PsaA}$ variant. Electron throughput was measured in isolated PS I complexes with phenazine methosulfate as the electron donor and flavodoxin (Flv) as the electron acceptor. The normalized rates were 325 μmol Flv mg Chl^{-1} hr^{-1} in the wild type, 147 μmol Flv mg Chl^{-1} hr^{-1} in the $M688H_{PsaA}$ variant and 269 μmol Flv mg Chl^{-1} hr^{-1} in the $M668H_{PsaB}$ variant (Fig. 4**D**). Given that there are ~100 Chl P_{700}^{-1} in cyanobacterial PS I, these rates corresponded to 9 e^- PS I^{-1} s^{-1}, 4 e^- PS I^{-1} s^{-1} and 7 e^- PS I^{-1} s^{-1}, respectively. The lower rates of electron throughput in the $M688H_{PsaA}$ and $M668H_{PsaB}$ variants imply that electron transfer is wholly or partially blocked in the A- and B-branches respectively. The slower growth of the $M688H_{PsaA}$ and $M668H_{PsaB}$ variant strains therefore appears to be a combination of a lower amount of PS I per cell as well as a lower electron transport throughput within each individual PS I complex.

3.3. Occupancy of the phylloquinone binding sites

The lower throughput of electrons in the variants could be due to either altered electron transfer kinetics or loss of phylloquinone from the binding site. Thus, we assayed the phylloquinone content of the PS I trimers. Our analysis showed that the $M688H_{PsaA}$ and $M668H_{PsaB}$ contained 94% and 103% of the phyloquinone content of the wild type when normalized to chlorophyll concentration. Both of these values are within the limits of error, indicating that the A_{1A} and A_{1B} sites in the $M688H_{PsaA}$ and $M668H_{PsaB}$ variants are fully occupied by phylloquinone.

3.4. Spin-polarized transient EPR spectroscopy at X-band

The room temperature spin-polarized transient EPR spectra of PS I complexes isolated from the wild type and the $M688H_{PsaA}$ and $M668H_{PsaB}$ variants are shown in Fig. 5. The spectra shown on the left have been extracted from time/field data sets at 220 ns, 360 ns and 1 μs after the laser flash. The right side of Fig. 5 shows transients taken at the field positions indicated by the corresponding arrows under the spectra. For wild type PS I, the E/A/E (E for emission and A for absorption) spin polarization pattern observed at 220 ns is derived primarily from the $P_{700}^+A_{1A}^-$ radical pair. The pattern evolves into the predominantly emissive spectrum at 1 μs, which is the P_{700}^+ contribution to the spectrum of $P_{700}^+(FeS)^-$ [32]. This spectrum then decays as a result of the loss of the spin polarization. Because the contribution

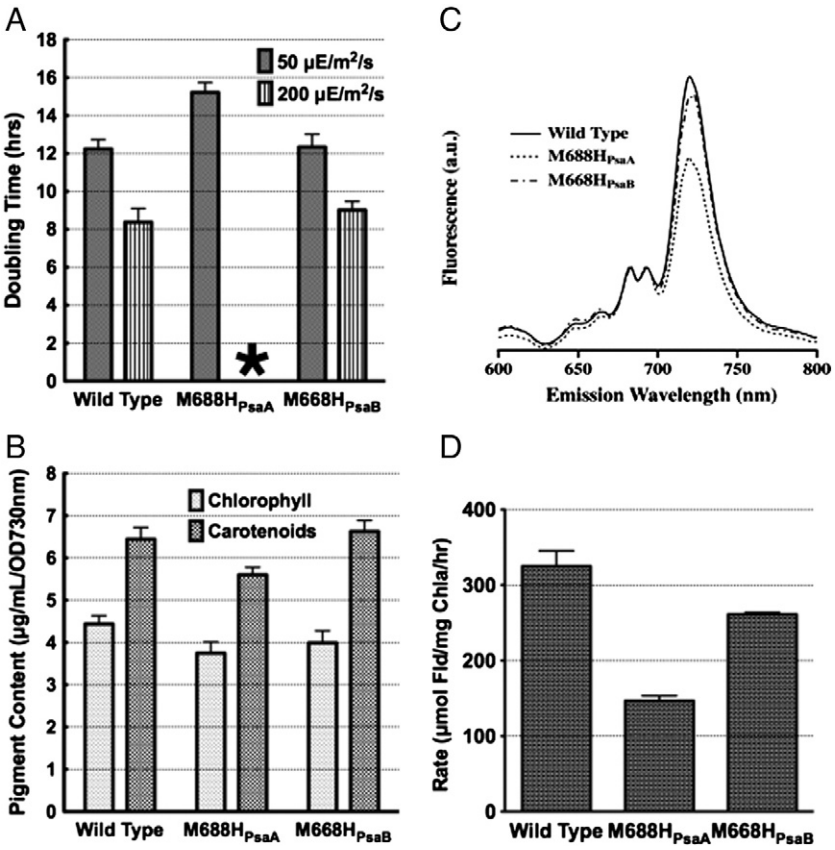

Fig. 4. Doubling time (A) and pigment content (B), whole cell 77 K fluorescence spectra (C) and flavodoxin photoreduction rates (D). Growth rates were measured for cultures grown under two light conditions, 50 μE/m^2/s (low light) and 200 μE/m^2/s (high light). The M688H$_{PsaA}$ strain showed no detectable growth under high light (*). The pigment content and 77 K fluorescence spectra were determined in cells grown under low light to 0.5 OD$_{730nm}$. Each data set was averaged from six biological duplicates. The flavodoxin photoreduction rates are depicted in units of μmols of flavodoxin reduced per mg of Chl *a* per hr. Each data set was averaged from five duplicates.

from the FeS cluster is not observed in the spectrum, we use the notation FeS to stand for any one of the F_X, F_A or F_B clusters. The fits of the transients from the wild type (Fig. 5, top right) yield a lifetime of 220 ns for electron transfer from A_{1A}^- to the FeS clusters and 1.4 μs for the decay of the polarization in agreement with previous EPR and optical studies [33–35]. Electron transfer from A_{1B}^- to F_X cannot be observed directly by EPR because it occurs within the rise time of the instrument. However, the fraction of B-branch electron transfer can be roughly estimated by the magnitude of the $P_{700}^+(FeS)^-$ contribution present at early time. For wild-type PS I, this fraction is ~15–20% [35].

An important feature of the spectrum of $P_{700}^+ A_{1A}^-$ is the prominent shoulder on the central absorptive peak. This shoulder arises from the *y*-component of the hyperfine splitting of the C3 methyl group protons and is sensitive to the spin density distribution on the semiquinone ring. In wild type PS I, the single H-bond to the C4 carbonyl group leads to asymmetry in the distribution such that the spin density is high on the ring carbon adjacent to the methyl group [36,37]. As a result, the *y*-component of the methyl hyperfine coupling is large and a shoulder is observed in the spectrum.

The corresponding transient EPR data of PS I from the M688H$_{PsaA}$ variant (Fig. 5, middle panels) are significantly different from those of the wild type (Fig. 5, top panels). First, the E/A/E pattern observed at early time does not evolve into the emissive $P_{700}^+(FeS)^-$ spectrum but decays with a lifetime of 1 μs. A study of the microwave power dependence of the decay (data not shown) indicates that it is due to the loss of spin polarization and not to electron transfer. Second, the amplitude of the spectrum is considerably lower than that of the wild type as can be inferred by the lower signal-to-noise ratio. Third, the spectrum lacks the prominent shoulder on the central absorptive peak. From these results we can conclude that in the M688H$_{PsaA}$ variant, the electron resides on A_{1A}^- for a time greater than a few μs, indicating that forward electron transfer occurs from A_{0A}^- to A_{1A} but electron transfer beyond A_{1A}^- to F_X is either slowed or blocked. The lower signal-to-noise ratio implies that the quantum yield of the $P_{700}^+ A_{1A}^-$ radical pair is reduced compared to the wild type. Further, the lack of the prominent shoulder on the central absorptive peak indicates a change in the spin density distribution on the quinone such that it is more symmetric. Such a change would be expected if the side chain of H688$_{PsaA}$ were to form an H-bond with the C1 carbonyl group of the phylloquinone as predicted by the MD simulations. The lack of a $P_{700}^+ FeS^-$ contribution suggests that the yield of B-branch electron transfer is small and/or it generates weak spin polarization. The loss of electron transfer to the iron-sulfur clusters cannot be a result of photo-reduction of the iron-sulfur clusters because if this were occurring, it would also be observed in the wild type.

In contrast, the transient EPR spectra of PS I from the M668H$_{PsaB}$ variant (Fig. 5, bottom panels) are similar to those of the wild type. However, if the transients of the M668H$_{PsaB}$ variant and the wild type are normalized to the same amplitude at field a, the absorptive part of the signal at field b is slightly larger in the M668H$_{PsaB}$ variant relative to the wild type. Such a difference would be expected if the contribution from $P_{700}^+(FeS)^-$ at early time was smaller in the M668H$_{PsaB}$ variant due to a decreased quantum yield of $P_{700}^+(FeS)^-$ from B branch electron transfer. Indeed, much more pronounced differences of this type have been observed previously in subunit deletion mutants in which the ratio of the fast and slow components of electron transfer from A_1 to F_X is strongly altered [35,38].

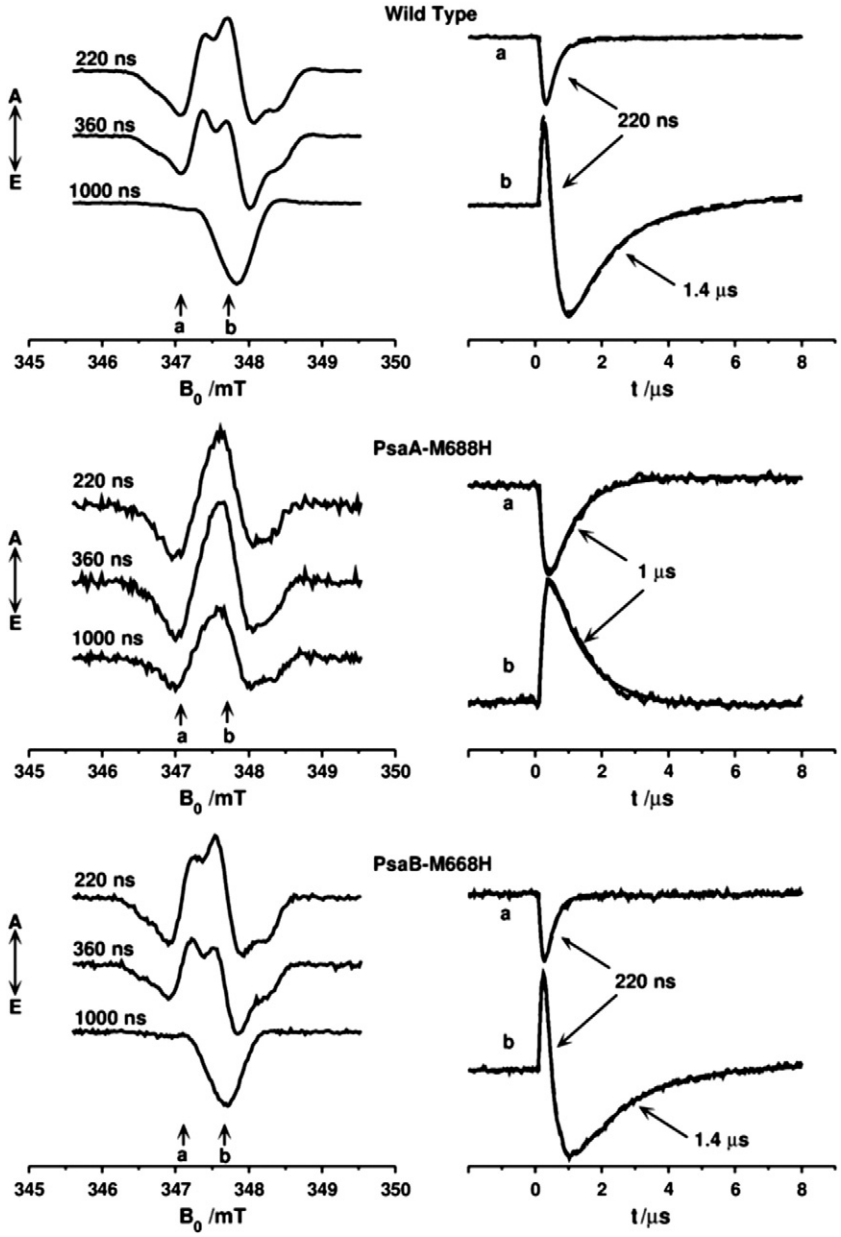

Fig. 5. Room temperature X-band spin-polarized transient EPR field-dependent spectra (**left**) **and time-dependent transients** (**right**). The spectra were extracted from the field/time data sets at the times indicated in the figure. The two arrows labeled a and b indicate the field positions at which the corresponding transients were taken. The labels A and E on the vertical axes indicate absorption and emission. The amplitudes of the spectra from the variants were normalized to the same amplitude as the wild type.

3.5. Time-resolved optical spectroscopy in the ns to s time range

We used time-resolved optical spectroscopy to determine the lifetimes of the A_{1A}^- and A_{1B}^- radicals and the relative use of the two branches more precisely. The measurements were carried out at 480 nm, a wavelength at which the electrochromic bandshift of the carotenoids located near A_{1A} and A_{1B} results in an absorbance increase when either of the two phylloquinones is reduced [39,40]. The electrochromic bandshift serves as a proxy that mirrors the transient redox changes of the phylloquinones. In wild type PS I the absorbance of phyllosemiquinone can be observed directly at 380 nm. However, measurement of the electrochromic bandshift at 480 nm eliminates complications due to spectral shifts of the phyllosemiquinone absorbance that might arise from alterations in the surroundings of the chromophore, including the presence of an additional hydrogen bond. Measurements at 480 nm differ from those at 380 nm in two ways. First, P_{700}^+ has a small absorption at this wavelength, hence, we complement these data with measurements at 820 nm, a wavelength that measures only absorbance changes due to P_{700}^+. Second, 480 nm light is actinic at the intensities used in this study, hence, we only fit data from 2 ns to 200 µs, a period of time in which the actinic effect has only a small influence (~5%) on the yield of charge separation (see Materials and methods and supporting information).

Figs. 6 and 7 show flashed-induced absorbance changes at 480 nm and 820 nm, respectively, in PS I from the wild type and the $M688H_{PsaA}$ and $M668H_{PsaB}$ variants. The data are presented on a logarithmic scale from 2 ns to 100 µs at 480 nm and from 2 ns to 2 s at 820 nm. The kinetics were decomposed using a stretched multiexponential fit, which reveals the lifetimes and amplitudes of the absorbance changes. The results of the data analysis described below are tabulated in Table 1.

In wild type PS I, three kinetic phases with lifetimes of 17.1 ns (0.62 mOD), 207 ns (1.18 mOD), and >10 µs (0.17 mOD) can be resolved at 480 nm (Fig. 6**A**). The residual (0.48 mOD) represents long-lived P_{700}^+ that does not decay on this timescale. The 17.1 ns and 207 ns

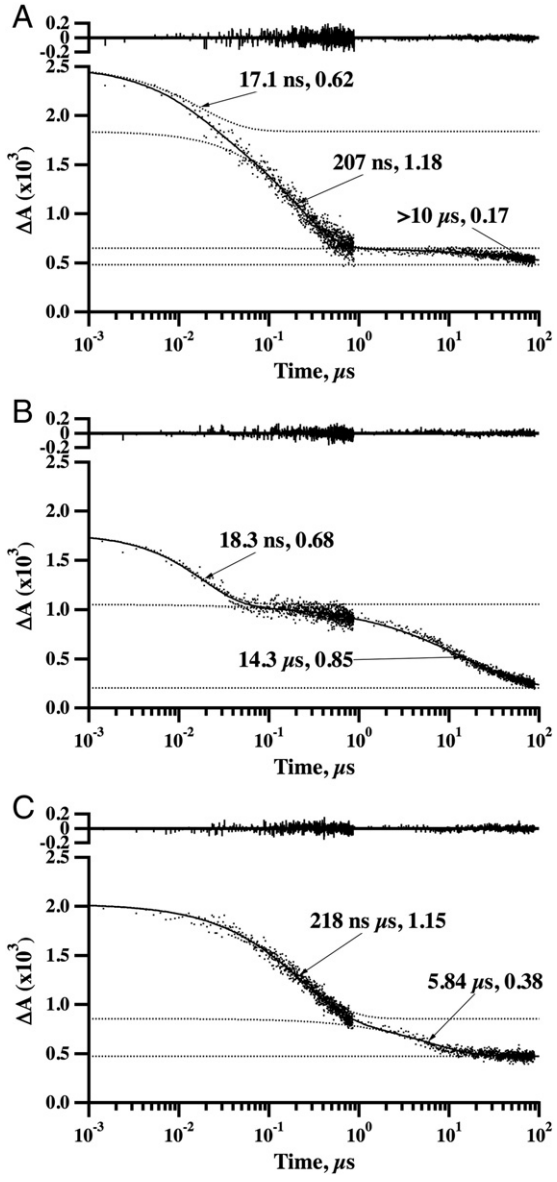

Fig. 6. Kinetics of flash-induced time-resolved absorbance changes at 480 nm for the wild-type (A), M688H$_{PsaA}$ variant (B) and M668H$_{PsaB}$ variant (C). The data sets from two different time resolutions were combined to resolve multiple kinetic phases. The absorbance values are plotted against the log-scaled time after the laser flash, and were stretched-fitted into a multi-exponential decay. The computer-generated fit is shown as a solid line. Each kinetic phase is presented with the lifetime and amplitude. The difference between experimental and fit values is plotted as a residual in the upper panel. The data sets were from 16 averages. The relative contributions of each kinetic phase can be judged by the intersection of the fit line with the abscissa.

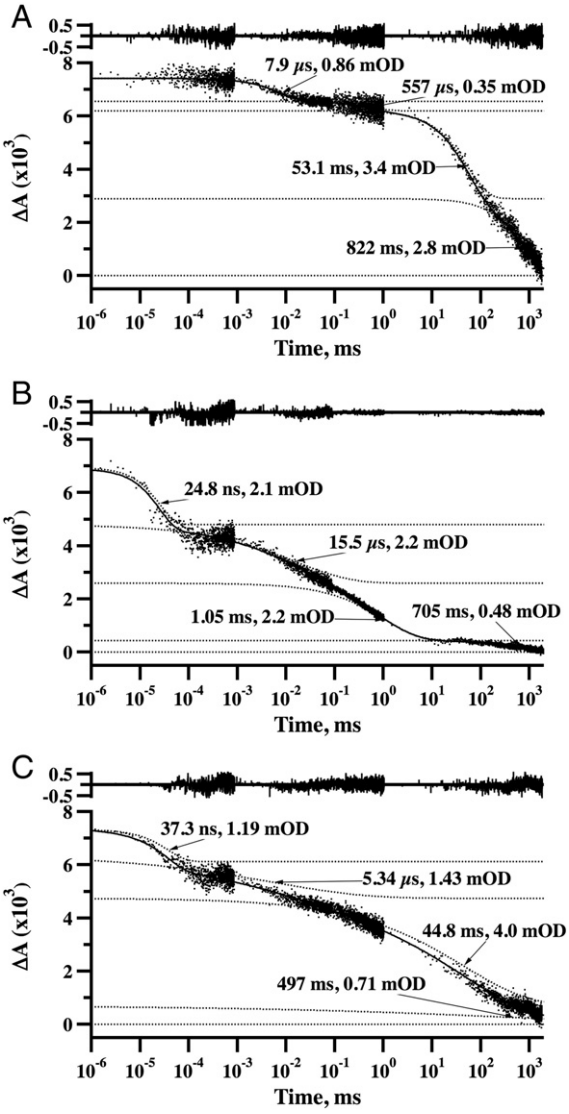

Fig. 7. Kinetics of flash-induced time-resolved absorbance changes at 820 nm for the wild-type (A), M688H$_{PsaA}$ variant (B) and M668H$_{PsaB}$ variant (C). The data sets from three different time resolutions were combined to resolve multiple kinetic phases. The absorbance values are plotted against the log-scaled time after the laser flash, and were stretched-fitted into a multi-exponential decay. The computer-generated fit is shown as a solid line. Each kinetic phase is presented with the lifetime and amplitude. The difference between experimental and fit values is plotted as a residual in the upper panel. The data sets were from 64 averages. The relative contributions of each kinetic phase can be judged by the intersection of the fit line with the abscissa.

components are assigned to electron transfer from A_{1B}^- to F_X and from A_{1A}^- to F_X, respectively by virtue of their lifetimes and in comparison with previous studies [7–9,41]. The ratio of ~1:2 for the absorbance change of the two kinetic phases is typical for B- and A-side electron transfer in PS I from *Synechocystis* sp. PCC 6803. The total absorbance change at 820 nm at the onset of the flash is 7.41 mOD (Fig. 7**A**), which is equivalent to 0.925 μM in P_{700} (80 μg Chl mL^{-1}), given an extinction coefficient of 8,000 M^{-1} cm^{-1} for P_{700}/P_{700}^+ at 820 nm. This corresponds to 97.2 Chl P_{700}^{-1}, which is in good agreement with the 96 Chl PS I^{-1} found in the X-ray crystal structure of PS I from *T. elongatus*.

Four kinetic phases with lifetimes of 7.9 μs (0.86 mOD), 557 μs (0.35 mOD), 53.1 ms (3.4 mOD) and 822 ms (2.8 mOD) can be resolved at 820 nm (Fig. 7**A**). The 7.9 μs component has a lifetime similar to the ~10 μs component observed at 480 nm. This signal arises from the recombination between A_{1A}^- or A_{1B}^- and P_{700}^+ in a fraction of PS I in which forward electron transfer beyond phylloquinone is impaired. The 557 μs component is characteristic of charge recombination between P_{700}^+ and F_X^- and arises from a fraction of PS I with damaged or reduced F_B and F_A clusters. The large 53.1 ms component is assigned to the well-characterized P_{700}^+ $[F_A/F_B]^-$ charge recombination and the 822 ms component to P_{700}^+ reduction by DCPIP in those reaction centers in which the electron on $[F_A/F_B]^-$ has been lost to dioxygen. At 480 nm (Fig. 6**A**), an absorption change of 1.8 mOD is contributed by the sum of the 17.1 ns and 207 ns components from A_{1A}^- and A_{1B}^-. The 0.48 mOD residual is contributed by P_{700}^+. Using these two values, we calculate that 79% of the absorbance change at 480 nm is due to A_{1A}^- and A_{1B}^-, and 21% is due to P_{700}^+. Because this ratio also applies to the ~10 μs kinetic phase, the total initial absorbance change of 2.45 mOD at 480 nm can be shown to be comprised of a sum total of 1.93 mOD from A_{1A}^- and A_{1B}^-, and 0.52 mOD from P_{700}^+. These values will be needed

Table 1
Compilation of data derived from the ns/μs/ms measurements.

480 nm			820 nm		
Lifetime	mOD	Assignment	Lifetime	mOD	Assignment
Wild type					
17.1 ns	0.62	$A_{1B}^- \rightarrow F_X$	7.9 μs	0.86	$A_1^- \rightarrow P_{700}^+$
207 ns	1.18	$A_{1A}^- \rightarrow F_X$	557 μs	0.35	$F_X^- \rightarrow P_{700}^+$
~10 μs	0.17	$A_{1A}^- \rightarrow P_{700}^+$	53.1 ms	3.40	$[F_A/F_B]^- \rightarrow P_{700}^+$
>100 μs	0.48	P_{700}^+	822 ms	2.80	DCPIP → P_{700}^+
Total	*2.45*		*Total*	*7.41*	
M688H$_{PsaA}$					
18.3 ns	0.68	$A_{1B}^- \rightarrow F_X$	24.8 ns	2.1	$A_{0A}^- \rightarrow P_{700}^+$
14.3 μs	0.85	$A_{1A}^- \rightarrow P_{700}^+$	15.5 μs	2.2	$A_{1A}^- \rightarrow P_{700}^+$
>100 μs	0.17	P_{700}^+	1.05 ms	2.2	$[F_A/F_B]^- \rightarrow P_{700}^+$
Total	*1.73*		705 ms	0.48	DCPIP → P_{700}^+
			Total	*6.98*	
M668H$_{PsaB}$					
218 ns	1.15	$A_{1A}^- \rightarrow F_X$	37.3 ns	1.19	$A_{0B}^- \rightarrow P_{700}^+$
5.84 μs	0.38	$A_{1B}^- \rightarrow P_{700}^+$	5.34 μs	1.43	$A_{1B}^- \rightarrow P_{700}^+$
>100 μs	1.48	P_{700}^+	44.8 ms	4.0	$[F_A/F_B]^- \rightarrow P_{700}^+$
Total	*2.01*		497 ms	0.71	DCPIP → P_{700}^+
			Total	*7.33*	

later to calculate quantum yields in the M688H$_{PsaA}$ and M668H$_{PsaB}$ variants.

In the M688H$_{PsaA}$ variant, two kinetic phases with lifetimes of 18.3 ns (0.68 mOD) and 14.3 μs (0.85 mOD) can be resolved at 480 nm (Fig. 6**B**). The residual (0.17 mOD) represents long-lived P_{700}^+ that does not decay on this timescale. Because the lifetime and amplitude of the 18.3 ns component are similar to that of the 17.1 ns component in wild type PS I (Fig. 6**A**), this kinetic phase is assigned to electron transfer from A_{1B}^- to F_X. The ~200 ns component characteristic of A-side electron transfer from A_{1A}^- to F_X is completely missing.

Four kinetic phases with lifetimes of 24.8 ns (2.1 mOD), 15.5 μs (2.2 mOD), 1.05 ms (2.2 mOD) and 705 ms (0.48 mOD) can be resolved at 820 nm (Fig. 7**B**), The 15.5 μs component is equivalent to the 14.1 μs component observed at 480 nm. Therefore, this kinetic phase arises from charge recombination of either A_{1A}^- or A_{1B}^- with P_{700}^+. Because forward electron transfer from A_{1B}^- to F_X is fully accounted for by the 18.3 ns component at 480 nm (Fig. 6**B**), the 15.5 μs event can be assigned to charge recombination between A_{1A}^- and P_{700}^+. Thus, electron transfer from A_{1A}^- to F_X is blocked in the M688H$_{PsaA}$ variant. Electron transfer along the unaltered B-branch to the FeS clusters is evident in the data at 480 nm, and the long-lived 705 ms kinetic phase, which is due to the reduction of P_{700}^+ by DCPIP, is present. It should be noted that the ~50 ms event characteristic of charge recombination between P_{700}^+ and $[F_A/F_B]^-$ is missing, and is replaced by a 1.05 ms event. This indicates that the backreaction from $[F_A/F_B]^-$ has been altered as a result of the mutation. The ~15 μs kinetic phase is due to charge recombination between A_{1A}^- and P_{700}^+; using the percentages extracted from the wild-type data at 480 nm, we calculate that of the 0.85 mOD, 0.67 mOD is from A_{1A}^- and 0.18 mOD is from P_{700}^+. In the wild type 1.18 mOD is from A_{1A}^-, hence, the quantum yield of forward electron transfer from A_{0A}^- to A_{1A} is 0.57. Thus, a little more than one-half of the electrons in the A-branch are transferred forward from A_{0A}^- to A_{1A} in the M688H$_{PsaA}$ variant.

The partial loss of forward electron transfer in the A-branch is reflected at 480 nm in the lower total amplitude of the absorption change at the onset of the flash (Fig. 6**B**) compared to the wild type (Fig. 6**A**). This could be due to either a failure to undergo charge separation or to charge separation followed by rapid recombination between P_{700}^+ and A_{0A}^-. Fig. 7**B** shows the presence of a 24.8 ns kinetic phase at 820 nm in the M688H$_{PsaA}$ variant, which is characteristic of the recombination between P_{700}^+ and A_0^- [42]. At 820 nm, the total absorbance at the onset of the flash is 7.0 mOD compared to 7.4 mOD in the wild type. This indicates that the quantum yield of charge separation between P_{700} and A_{0A} is virtually unaffected by the mutation.

In the M668H$_{PsaB}$ variant, two kinetic phases with lifetimes of 218 ns (1.15 mOD) and 5.84 μs (0.38 mOD) can be resolved at 480 nm (Fig. 6**C**). The residual (1.48 mOD) represents long-lived P_{700}^+ that does not decay on this timescale. Because the lifetime and amplitude of the 218 ns component is similar to the 207 ns component in wild type PS I (Fig. 6**A**), this kinetic phase is assigned to electron transfer from A_{1A}^- to F_X. The ~20 ns component characteristic of B-side electron transfer from A_{1B}^- to F_X is completely missing.

Four kinetic phases are resolved with lifetimes of 37.3 ns (1.19), 5.34 μs (1.43 mOD), 44.8 ms (4.0 mOD) and 497 ms (0.71 mOD) at 820 nm (Fig. 7**C**). The 5.34 μs component is equivalent to the 5.84 μs component seen at 480 nm. Therefore, this kinetic phase is assigned to charge recombination between either A_{1A}^- or A_{1B}^- and P_{700}^+. Because forward electron transfer from A_{1A}^- to F_X is fully accounted for by the 218 ns component at 480 nm (Fig. 6**C**), the ~5 μs event can be assigned to charge recombination between A_{1B}^- and P_{700}^+. Thus, electron transfer from A_{1B}^- to F_X is blocked in the M668H$_{PsaB}$ variant. The 44.8 ms (4.0 mOD) and the 497 ms (0.71 mOD) kinetic phases are characteristic of charge recombination between P_{700}^+ and $[F_A/F_B]^-$ and reduction of P_{700}^+ by DCPIP, respectively. In contrast to the corresponding A-branch mutation M688H$_{PsaA}$, which changes the lifetime of the P_{700}^+ $[F_A/F_B]^-$ backreaction, the B-branch mutation M688H$_{PsaA}$ does not influence the kinetics of the recombination from the terminal iron sulfur clusters. With the ~5 μs kinetic phase assigned to charge recombination between A_{1B}^- and P_{700}^+ and using the relative absorbance changes for A_1^- and P_{700}^+ extracted from the wild-type data at 480 nm, we calculate that of the 0.38 mOD associated with the ~5 μs phase, 0.30 mOD is due to A_{1B}^- and 0.08 mOD is due to P_{700}^+. In the wild type, 0.62 mOD is due to A_{1B}^-, hence, the quantum yield of forward electron transfer A_{1B} is 0.48. Thus, a little less than one-half of the electrons in the B-branch are transferred forward from A_{0B}^- to A_{1B} in the M668H$_{PsaB}$ variant.

The partial loss of forward electron transfer to A_{1B} in the B-branch is reflected at 480 nm in the lower total amplitude at the onset of the flash (Fig. 6**C**) compared to the wild type (Fig. 6**A**). This could be due to either a failure to undergo charge separation or to charge separation followed by rapid recombination between P_{700}^+ and A_{0B}^-. Fig. 7**C** shows the presence of a 37.3 ns (1.19 mOD) kinetic phase at 820 nm in the M668H$_{PsaB}$ variant, which is characteristic of the recombination between P_{700}^+ and A_0^- [42]. At 820 nm, the total absorbance at the onset of the flash is 7.0 mOD compared to 7.4 mOD in the wild type, indicating that the quantum yield of charge separation between P_{700} and A_{0B} is virtually unaffected by the mutation.

3.6. Spin-polarized P_{700} triplet from radical pair recombination

In PS I, triplet states can be generated as a result of two processes: intersystem crossing and charge recombination. The former occurs when energy transfer from the antenna Chls to the trapping center is inefficient and results in a population of Chl and carotenoid triplet states. Charge recombination populates the triplet state of P_{700} ($^3P_{700}$) when electron transfer past A_0 is blocked. In transient EPR experiments, $^3P_{700}$ is easily distinguished from other types of triplets by its zero-field splitting parameters and characteristic AEEAAE polarization [43–45]. Fig. 8 shows spin polarized EPR spectra of the wild type and the M688H$_{PsaA}$ and M668H$_{PsaB}$ variants at 80 K in the field region where triplet states contribute. The strong truncated peaks in the center of the spectra around 345 mT in all three samples represent the $P_{700}^+A_1^-$ radical pair. The dashed spectra are simulations. The wild-type spectrum shows only a very weak, broad E/A pattern that can be simulated as a chlorophyll triplet populated by intersystem crossing. In contrast, the M688H$_{PsaA}$ and M668H$_{PsaB}$ variants show clearly defined spectra, which are simulated well with the characteristic AEEAAE pattern of $^3P_{700}$ formed by recombination of $P_{700}^+A_0^-$. Thus, these spectra confirm blockage of electron transfer past A_0 in the two variants. The amplitude of the $^3P_{700}$ spectrum in the M688H$_{PsaA}$ variant is 3.5 times larger than in the M668H$_{PsaB}$ variant. This agrees qualitatively with

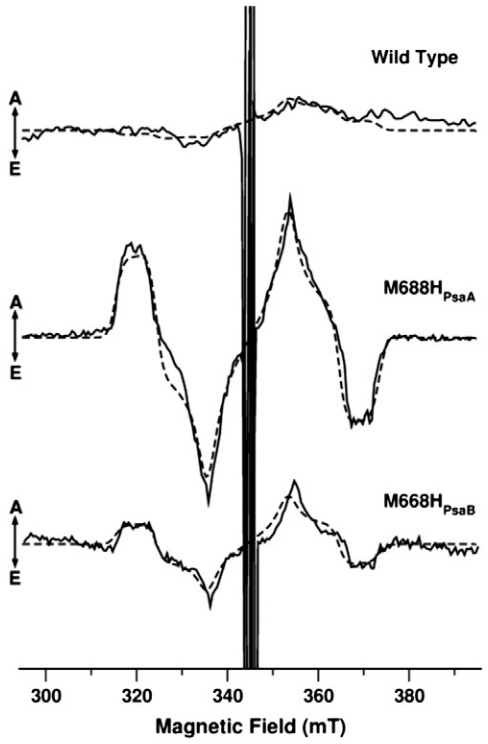

Fig. 8. Spin polarized transient EPR spectra of the excited triplet state of P_{700}. The solid curves are the experimental data and the dashed curves are simulations. The off-scale peaks in the center of the spectrum arise from the radical pair $P_{700}^{+}A_1^{-}$. The zero-field splitting parameters used in the simulation are $|D| = 250 \times 10^{-4}\ cm^{-1}$ and $|E| = 32 \times 10^{-4}\ cm^{-1}$. For the wild type intersystem crossing was assumed to populate the triplet sublevels according to their *z*-character. For the two variants the triplet was assumed to be formed by charge recombination so that only the T_0 triplet sublevel is populated.

the relative amplitudes of the 30 ns phase in the room temperature optical data, supporting the assignment of this phase to charge recombination between P_{700}^{+} and A_0^{-}. When the PS I samples were incubated with a 100-fold excess of phylloquinone only minor changes in the amplitude of the ^{3}P700 were observed (data not shown) confirming that the binding sites are fully occupied and that the charge recombination between P_{700}^{+} and A_0^{-} is not the result of loss of phylloquinone.

3.7. Ultrafast studies of the formation of the primary and secondary radical pairs

Fig. 9 shows ultrafast transient spectra for PS I complexes from the wild type and the M688H$_{PsaA}$ and M668H$_{PsaB}$ variants obtained at a 5 ps and 500 ps delay following a 20 fs exciting pulse centered at 720 nm. The most prominent feature in all of the spectra is the bleaching of the Chl Soret band and Q_y-band around 450 and 700 nm, respectively. At 5 ps, the spectra of wild type (Fig. 9**A**), the M688H$_{PsaA}$ variant (Fig. 9**C**) and the M668H$_{PsaB}$ variant (Fig. 9**E**) are similar and show an isosbestic point (zero crossing) in the Soret region around 460 nm, absorption increase maxima at approximately 480, 510, 620 and 660 nm, and absorption decrease troughs at 690 and 705 nm. Recently, it was shown that the primary charge separation process $P_{700}{}^{*}A_0 \rightarrow P_{700}^{+}A_0^{-}$ is extremely fast and occurs within 100 fs [5]. Thus, the similarity of the spectra of the wild type and M688H$_{PsaA}$ and M668H$_{PsaB}$ variants at 5 ps implies that the $P_{700}{}^{*}A_0 \rightarrow P_{700}^{+}A_0^{-}$ transition is also very fast in the two variants.

In contrast, at 500 ps, the spectra of the wild type (Fig. 9**B**), the M688H$_{PsaA}$ variant (Fig. 9**D**), and the M668H$_{PsaB}$ variant (Fig. 9**F**) differ from one another. In the wild type, a sharp trough at 465 to 470 nm, an isosbestic point around 575 nm, a broad negative band between 575 and 660 nm, and an asymmetric, negative-positive-negative feature in the Q_y-region are observed. In the M688H$_{PsaA}$ variant, the corresponding spectrum does not exhibit the sharp trough around 460 nm, the isosbestic point is shifted from 590 to 600 nm, and the broad negative band is shifted between 600 and 650 and the local maximum at 694 nm are less pronounced than in the wild type. In the M668H$_{PsaB}$ variant, the dip around 460 nm is present, and the positions and intensities of the isosbestic point, the broad negative band between 600 and 650, and the local maximum at 694 nm lie between those of the wild-type and the M688H$_{PsaA}$ variant, but are markedly closer to that of the wild-type. Previous studies have shown that under similar experimental conditions, the lifetime of antenna excited states is ~5 ps [5]. Thus, the changes in the absorbance difference spectra between 5 ps and 500 ps are primarily the result of electron transfer from A_0^{-} to A_1. For wild type PS I, the spectrum at 5 ps is mostly due to $P_{700}^{+}A_0^{-}$ while the spectrum at 500 ps can be assigned to $P_{700}^{+}A_1^{-}$. It appears that in the M688H$_{PsaA}$ and M668H$_{PsaB}$ variants some of the $P_{700}^{+}\,A_0^{-}$ spectrum is still present at 500 ps, but that the amount of this contribution is larger in the M688H$_{PsaA}$ variant. This agrees with the ns measurements shown in Fig. 7**B** and **C**.

The lifetime and yield of electron transfer past A_0 can be estimated from the time and wavelength-dependent absorbance change data $\Delta A(\lambda,t)$ provided the following assumptions are made. (i) Changes to the transient spectrum of $P_{700}^{+}\,A_1^{-}$ as a result of the mutations in the M688H$_{PsaA}$ and M668H$_{PsaB}$ variants are negligible; accordingly, the spectrum of the wild type taken at 500 ps after the pump flash can be used in the kinetic decompositions for the two variants. (ii) Contributions to the time dependence of the spectra due to energy transfer are negligible; accordingly, in wild type PS I, the spectrum at 5 ps should evolve into the spectrum at 500 ps with a single time constant associated with electron transfer from A_0^{-} to A_1. Spectra at intermediate time points should therefore be a linear combination of the 5 ps and 500 ps spectra. We have fit the data for each sample with the following expression:

$$\Delta\mathbf{A}^{\mathrm{WT,M688H\ or\ M668H}}(\lambda,t) = c_1(t)\cdot\Delta\mathbf{A_1}^{\mathrm{WT,M688H\ or\ M668H}}(\lambda) + c_2(t)\cdot\Delta\mathbf{A_2}^{\mathrm{WT}}(\lambda),$$

where $\mathbf{\Delta A_1}(\lambda)$, $\mathbf{\Delta A_2}(\lambda)$ represent the normalized spectra at 5 ps and 500 ps delays and $\boldsymbol{c_1}(t)$, $\boldsymbol{c_2}(t)$ represent the populations of the corresponding states. The spectra were normalized relative to the same concentration of excited PS I. For the wild type and the two variants the shapes of spectra at 5 ps delay are similar and $\mathbf{\Delta A_1}(\lambda)$ represents the spectrum of $P_{700}^{+}A_0^{-}$. However, at 500 ps, the spectra of the three samples differ. The difference is explained by different concentrations of the states $P_{700}^{+}A_0^{-}$ ($\boldsymbol{c_1}$) and $P_{700}^{+}A_1^{-}$ ($\boldsymbol{c_2}$) at 500 ps delay. In the case of the wild type, we assume that this spectrum represents $P_{700}^{+}A_1^{-}$. Thus, the kinetics of the $P_{700}^{+}A_0^{-} \rightarrow P_{700}^{+}A_1^{-}$ electron transfer were determined by using the $\mathbf{\Delta A_2}(\lambda, t = 500\ ps)$ of WT and $\mathbf{\Delta A_1}^{\mathrm{WT,\ AMH\ or\ BMH}}$ (λ, t = 5 ps) (spectra from data sets of wild type, M688H$_{PsaA}$ and M668H$_{PsaB}$, respectively).

The coefficients $\boldsymbol{c}_1(t)$ and $\boldsymbol{c}_2(t)$ are shown in Fig. 10 as a function of time. In the wild type (Fig. 10**A**), the coefficient of the early spectrum decays from one to zero, and the coefficient of the late spectrum rises from zero to one. Both curves are well described by a single exponential with a time constant of ~26 ps, consistent with previously reported lifetimes for electron transfer from A_0^{-} to A_1 [46]. In the M688H$_{PsaA}$ variant (Fig. 10**B**), the kinetics of $A_0^{-} \rightarrow A_1$ electron transfer are clearly biexponential but the lifetime of the major component is the same as in the wild type. At late time $c_1 \approx 0.29$, reflecting the lack of $A_0^{-} \rightarrow A_1$ electron transfer in ~30% of the PS I complexes. The total normalized amplitude at 500 ps, $A_{tot} = c_1(t = 500\ ps) + c_2(t = 500\ ps) < 1$.

This suggests that the yield of charge recombination within the first 500 ps may be higher in M688H$_{PsaA}$ variant than in the wild type or M668H$_{PsaB}$ variant. The difference of the A_{tot} values between the wild type and M668H$_{PsaB}$ variant is negligible in the subnanosecond time range. Qualitatively this observation corresponds to the results of time-resolved optical spectroscopy in the ns to s time range (Fig. 6

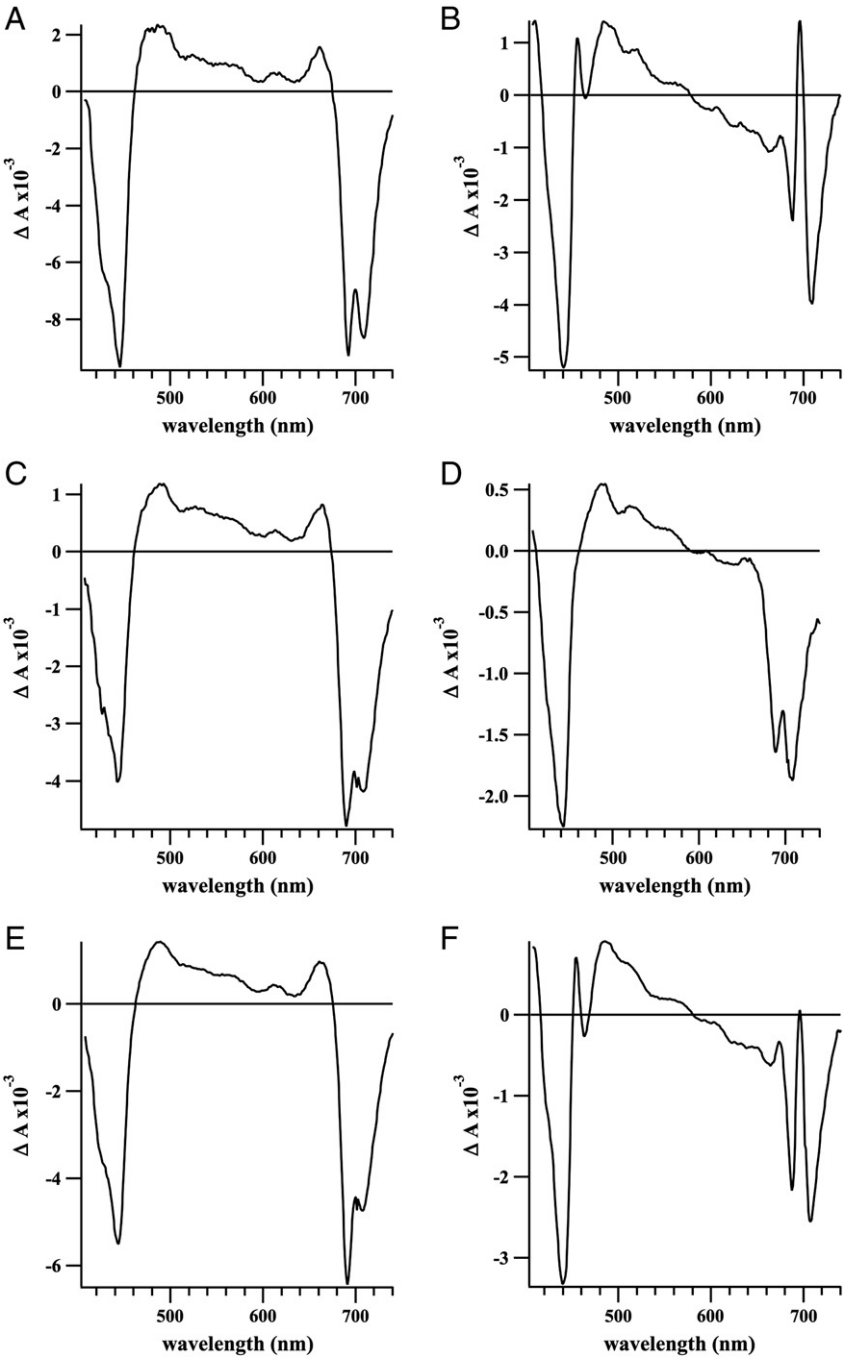

Fig. 9. Transient absorption spectra of the PS I complexes from the wild-type (**A**), **M688H$_{PsaA}$ variant** (**B**), **and M668H$_{PsaB}$ variant** (**C**) **at 5 ps and 500 ps delay times**. A description of the methodology is provided in the Materials and Methods section.

and 7), where the yield of radical states in the M688H$_{PsaA}$ variant is lower.

In the M668H$_{PsaB}$ variant (Fig. 10**C**), the same lifetime is obtained but the transition is not complete. At late times $c_1 \approx 0.09$, suggesting that forward electron transfer past A_0 is blocked in ~10% of the PS I complexes. The values of c_1 at late time in the variants are in reasonable agreement with the findings of the ns study (Table 1), which shows that the $A_0^- \rightarrow P_{700}^+$ charge recombination represents 30% of the total absorbance change in the M688H$_{PsaA}$ variant, whereas it represents 16% of the total absorbance change in the M668H$_{PsaB}$ variant.

The data derived from fs/ps measurements are compiled in Table 2. The kinetics in the wild-type sample can be approximated by a single exponential with $\tau_1 = 26$ ps. Since the ns data clearly show kinetic phases corresponding to electron transfer in the two branches, the monophasic fs/ps kinetics indicate that the rates of electron transfer from A_{0A}^- to A_{1A} and from A_{0B}^- to A_{1B} must be similar in the wild type, in agreement with previous ultrafast results [16]. In this case, the similar kinetic phase ($\tau_1 = 25$ ps, $A_1 = 86\%$) observed in the M668H$_{PsaB}$ variant can be attributed to electron transfer in the non-mutated A-branch. The slower kinetic component with $\tau_2 = 250$ ps ($Y_0 = 7\%$) can be attributed

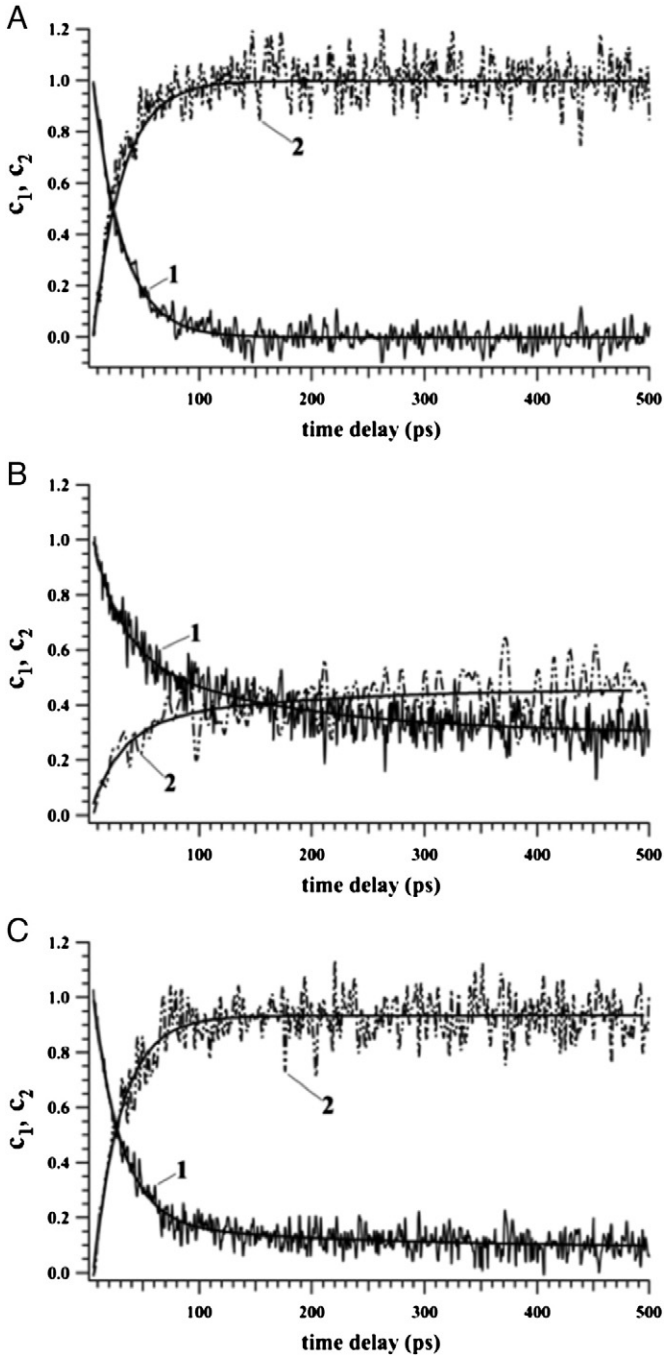

Fig. 10. Decomposition of the absorption difference spectra into contributions from $P_{700}^{+}A_0^{-}$ and $P_{700}^{+}A_1^{-}$. The traces are the amplitudes $c_1(t)$ and $c_2(t)$ obtained by fitting the time/wavelength data with $S(t,\lambda) = c_1(t)\,A_1(\lambda) + c_2(t)\,A_2(\lambda)$, where $A_1(\lambda)$ and $A_2(\lambda)$ are the normalized absorption difference spectra of $P_{700}^{+}A_0^{-}$ and $P_{700}^{+}A_1^{-}$, respectively. Trace 1 shows the disappearance of $P_{700}^{+}A_0^{-}$; trace 2 shows formation of $P_{700}^{+}A_1^{-}$. A) Wild type PS I, a monoexponential fit to the amplitudes gives $\tau_{c1} = 26$ ps, $\tau_{c2} = 31$ ps; B) $M688H_{PsaA}$ a biexponential fit gives $\tau_1 = 25$ ps ($a_1 = 44\%$), $\tau_2 = 145$ ps ($a_2 = 29\%$) and a long-lived component ($Y_0 = 27\%$), C) $M668H_{PsaB}$, a monoexponential fit gives $\tau_{c1} = 26$ ps, $\tau_{c2} = 29$ ps.

Table 2
Compilation of data derived from the fs/ps measurements.

Species	Y_0, %	τ_1, ps	A_1, %	τ_2, ps	A_2, %
Wild type	0	26	100	-	-
BMH	7	25	86	250 ± 50	7
AMH	27	26	44	150 ± 25	29

to electron transfer in the impaired B-branch, while the long-lived component represented by Y_0 (7%) likely results from the fraction of complexes in which the electron transfer from A_{0B}^{-} to A_{1B} in the impaired B branch is blocked. Similarly, in the $M688H_{PsaA}$ variant, the fast kinetic component ($\tau_1 = 26$ ps, $A_1 = 44\%$) can be attributed to electron transfer in the non-mutated B-branch. The slower component ($\tau_2 = 150$ ps, $A_2 = 29\%$) can be attributed to electron transfer in the impaired A-branch, while the long-lived component represented by Y_0 ($Y_0 = 27\%$) can be assigned to the fraction of PS I complexes in which the electron transfer from A_{0A}^{-} to A_{1A} along the impaired A branch is blocked.

4. Discussion

When a His is substituted for $M688_{PsaA}/M668_{PsaB}$ in PS I, the imidazole nitrogen atoms appear to be in a position to provide a bond to A_{0A}/A_{0B} and to A_{1A}/A_{1B}. Indeed, all of the low energy conformations found in the modeling studies have the ε-nitrogen of $His688_{PsaA}$ coordinated to A_{0A}. In contrast, a wide distribution of possible distances between the δ-nitrogen and the C1 carbonyl oxygen is found. The experimental results are consistent with this picture and reveal that the substitution of His for Met in *Synechocystis* sp. PCC 6803 results in two populations of PS I. In the $M688H_{PsaA}$ variant, about one half of the electrons taking the A-branch recombine with P_{700}^{+} from A_{0A}^{-} and the other half recombine from A_{1A}^{-}. The remaining absorption change at 820 nm (2.68 mOD) is due to unaltered B-side electron transfer. The latter represents 38% of the total absorption change at 800 nm, a value that agrees well with 34% of the absorption change at 480 nm attributed to B-side electron transfer (Table 1). In the $M668H_{PsaB}$ variant, about one half of the electrons taking the B-branch recombine with P_{700}^{+} from A_{0B}^{-} and the other half recombine from A_{1B}^{-}. The remaining absorption change at 820 nm (4.71 mOD) is due to unaltered A-side electron transfer. This represents 62% of the total absorption change at 820 nm, a value that agrees well with the 66% absorption change at 480 nm attributed to A-side electron transfer (Table 1).

Thus, in one population, the electron on A_0^{-} does not proceed forward to A_1 in the affected branch, but instead recombines with P_{700}^{+}. Based on the results of His variants in *C. reinhardtii* (as well as the previous study of *Synechocystis* sp. PCC 6803 [22]), this observation can be attributed to the presence of a coordination bond between the imidazole nitrogen and A_0. One reason for the lack of forward electron transfer in the His variants may be that the midpoint potential of the A_0^{-}/A_0 couple has become higher than the A_1^{-}/A_1 couple. The bond between His and A_0 would withdraw electron density from the ring, thereby stabilizing the Chl radical anion relative to the ground state and raising its midpoint potential. Because of their low values, the midpoint potentials of A_0 and A_1 are not known with certainty. For the purpose of this discussion, we employ the values determined using semi-continuum electrostatic methods [47]. The difference between the midpoint potentials of A_{0A} (-1.271 V) and A_{1A} (-0.671 V) and between A_{0B} (-1.314 V) and A_{1B} (-0.844 V) would mean that the substitution of Met for His would result in an increase of at least 600 mV and 470 mV in the midpoint potentials of A_{0A} and A_{0B}, respectively (assuming no effect on A_{1A} or A_{1B}). Recent theoretical studies on Met to Asn variants of PS I indicates that an increase in reduction potential of as much as 300 mV is possible when the Asn N is the ligand to A_0 [48]. Either the midpoint potential has changed by a large amount by virtue of the altered coordination bond or additional factors such as a change in the electronic coupling are present that contribute to the loss of forward electron transfer between A_0 and A_1.

In the second population, the electron on A_0 is transferred to A_1 in the affected branch, but not further to the Fe/S clusters. In this population, the electron on A_{1A}^{-} and A_{1B}^{-} recombines with P_{700}^{+} with lifetimes of 15 μs and 5 μs, respectively. The transient EPR study shows that in this population the spin density distribution on the phyllosemiquinone is more symmetric than in wild type PS I, and this difference is most

probably the result of an H-bond between the imidazole δ-nitrogen and the C1 carbonyl oxygen. The presence of this H-bond would stabilize the semiquinone anion radical relative to the ground state, thereby raising its midpoint potential beyond that of F_X. It is not straightforward to estimate the change in quinone potential that would prevent forward electron transfer to F_X. However, the kinetics observed in the *menB* variant provide a useful reference in this regard. In this variant plastoquinone-9 is incorporated into the A_{1A} and A_{1B} sites [24,49]. Forward electron transfer from A_{1A} and A_{1B} to F_X occurs with 1/*e* times of ~20 μs and ~200 μs, respectively, and the backreaction between P_{700}^+ and $[F_A/F_B]^-$ occurs with a 1/*e* time of 3 ms [50]. In DMF solution, the reduction midpoint potential of plastoquinone is ~100 mV more positive than that of phylloquinone [51,52]. Although the midpoint potential of plastoquinone-9 in the A_{1A} and A_{1B} binding sites is not known, we can nonetheless surmise that raising the quinone potential by ~100 mV would slow forward electron transfer lifetime into the tens to hundreds of microseconds range. In the $M688H_{PsaA}$ and $M688H_{PsaB}$ variants the forward electron transfer lifetime must be greater than the 15 μs and 5 μs backreaction lifetimes. Hence, we can conclude that in the absence of any other changes, the H-bond to His would need to stabilize the quinone by more than ~100 mV. A recent comparison of the midpoint potentials of several quinones in protic and aprotic solvents shows that the stabilization due to H-bonding in a protic environment is in the range of 200 to 300 mV [53]. Thus, the shift in potential needed to block forward electron transfer past A_1 in PS I is within the expected range for the contribution of an H-bond to the stabilization of a semiquinone radical. It should be noted that in this population of PS I, the molecular mechanics calculations indicate that His would also be coordinated to A_0. While this would otherwise lead to a recombination between P_{700}^+ and A_0^-, the added presence of the H-bond bond between the His and the phylloquinone would raise the midpoint potential of A_1. The data show that this is sufficient to permit forward electron transfer from A_0^- to A_1. At the same time, the increase in the midpoint potential of A_1 would prevent electron transfer to F_X. No electron transfer to the Fe/S clusters would occur either in the population of reaction centers in which His is only coordinated to A_0 or in the population of reaction centers in which His is additionally H-bonded to A_1.

The ultrafast data are consistent with unequal A- and B-branch electron transfer. If we consider only the contribution from the fast 26 ps phase, then the ratio between A and B-branch electron transfer would be 86%/44% = 1.95. If we consider the sum of the relative contributions of the slow and long-lived components, which according to our assessment represent the impaired branch contribution, then the ratio would be (29% + 27%)/(7% + 7%) = 4. Thus our data support previous assessments that at room temperature electron transfer in PS I from *Synechocystis* sp. PCC 6803 is asymmetric [19], with 66% to 80% contributed by the A-branch and 20% to 34% contributed by the B-branch. This conclusion is mirrored in the flavodoxin reduction studies, which show a significantly greater loss of electron transfer throughput in the $M688H_{PsaA}$ variant than in the $M668H_{PsaB}$ variant. This makes it possible for both variants to grow under low light conditions despite the fact that electron transfer to the FeS clusters is blocked in the branch carrying the mutation. A similar phenotype was shown in Met to His variants of PS I from *C. reinhardtii* [12]. However, the corresponding $M688H_{PsaA}$ and $M668H_{PsaB}$ variants accumulated to wild type levels under low-light conditions and were light sensitive, and opposite to its cyanobacterial counterpart, the $M668H_{PsaB}$ strain rather than the $M688H_{PsaA}$ strain failed to grow under a high light regime.

There is no significant loss of quantum yield of primary charge separation in either variant. The amplitude of the 200 ns kinetic phase was unaltered in the $M668H_{PsaB}$ variant, and the amplitude of the 20 ns kinetic phase was unaltered in the $M688H_{PsaA}$ variant, but the yield of electron transfer to the FeS clusters was reduced as a result of these changes. Thus, in the $M688H_{PsaA}$ and $M668H_{PsaB}$ variants in *Synechocystis* sp. PCC 6803 the presence of a second branch does not allow wild type levels of electron throughput to be maintained, *i.e.* the electrons are not re-routed through the alternative branch, but it does permit sufficient throughput to allow the organisms to grow under low light conditions.

Another interesting finding is that the charge recombination kinetics between $[F_A/F_B]^-$ to P_{700}^+ has been altered in the $M688H_{PsaA}$ variant ($1/e = 1.05$ ms), but not in the $M66H_{PsaB}$ variant (1/e = 44.8 ms) relative to the wild-type (1/e = 53.1 ms). These data imply that the charge recombination pathway in PS I occurs along the A- rather than B-branch of cofactors. This pathway makes sense energetically: the electron should favor the $F_X \rightarrow A_{1A}$ route, which is thermodynamically downhill, rather than the $F_X \rightarrow A_{1B}$ route, which is thermodynamically uphill.

We note that ENDOR and/or ESEEM experiments in which the hyperfine coupling to the H-bonded proton can be directly observed will be important to confirm the formation of an H-bond between His and A_{1A} and to A_{1B} and to give a clearer picture of the strength and the disorder of the H-bonding. We also note that the behavior we observe here for *Synechocystis* sp. PCC 6803 has not been reported for the corresponding PS I variants of *C. reinhardtii*. In a forthcoming article we will present a direct comparison of the behavior of the variants of the two species will show that a clear difference exists between them.

Acknowledgments

The authors thank Mr. Fedor Gostev and Dr. Mahir Mamedov for their participation in several of the experiments. This work was funded by grants from the US National Science Foundation (MCB-1021725), the Russian Foundation for Basic Research (RFBR 12-04-00821, 13-04-40299-H, 13-04-40298-H, 14-03-31370), the Civilian Research and Development Foundation (CRDF RUB1-7029-MO-11), the Natural Sciences and Engineering Research Council of Canada, and the Louisiana Board of Regents award (NSF(2010)-PFUND-217).

Appendix A. Supplementary data

Supplementary data to this article can be found online at http://dx.doi.org/10.1016/j.bbabio.2014.04.004.

References

[1] S. Sadekar, J. Raymond, R.E. Blankenship, Conservation of distantly related membrane proteins: photosynthetic reaction centers share a common structural core, Mol. Biol. Evol. 23 (2006) 2001–2007.
[2] P. Jordan, P. Fromme, H.T. Witt, O. Klukas, W. Saenger, N. Krauß, Three dimensional structure of Photosystem I at 2.5 Å resolution, Nature 411 (2001) 909–917.
[3] T. Watanabe, M. Kobayashi, A. Hongu, M. Nakazato, T. Hiyama, N. Murata, Evidence that a chlorophyll *a*′ dimer constitutes the photochemical reaction center 1 (P700) in photosynthetic apparatus, FEBS Lett. 191 (1985) 252–256.
[4] J. Golbeck, Photosystem I: the light-driven plastocyanin:ferredoxin oxidoreductase, Springer, Dordrecht, 2006.
[5] I.V. Shelaev, F.E. Gostev, M.D. Mamedov, O.M. Sarkisov, V.A. Nadtochenko, V.A. Shuvalov, A.Y. Semenov, Femtosecond primary charge separation in *Synechocystis* sp. PCC 6803 photosystem I, Biochim. Biophys. Acta 1797 (2010) 1410–1420.
[6] S. Savikhin, W. Xu, P. Martinsson, P.R. Chitnis, W.S. Struve, Kinetics of charge separation and A0- → A1 electron transfer in Photosystem I reaction centers, Biochemistry 40 (2001) 9282–9290.
[7] N. Srinivasan, J.H. Golbeck, Protein-cofactor interactions in bioenergetic complexes: the role of the A(1A) and A(1B) phylloquinones in Photosystem I, Biochim. Biophys. Acta 1787 (2009) 1057–1088.
[8] K. Brettel, Electron transfer from A_1^- to an iron-sulfur center with $t_{1/2} = 200$ ns at room temperature in Photosystem I. Characterization by flash absorption spectroscopy, FEBS Lett. 239 (1988) 93–98.
[9] P. Setif, H. Bottin, Identification of electron-transfer reactions involving the acceptor A1 of photosystem I at room temperature, Biochemistry 28 (1989) 2689–2697.
[10] K. Sauer, P. Mathis, S. Acker, J.A. Van Best, Electron acceptors associated with P-700 in Triton solubilized photosystem I particles from spinach chloroplasts, Biochim. Biophys. Acta 503 (1978) 120–134.
[11] I.R. Vassiliev, Y.S. Jung, M.D. Mamedov, A. Semenov, J.H. Golbeck, Near-IR absorbance changes and electrogenic reactions in the microsecond-to-second time domain in Photosystem I, Biophys. J. 72 (1997) 301–315.
[12] W.V. Fairclough, A. Forsyth, M.C. Evans, S.E. Rigby, S. Purton, P. Heathcote, Bidirectional electron transfer in Photosystem I: electron transfer on the PsaA side is not

essential for phototrophic growth in *Chlamydomonas*, Biochim. Biophys. Acta 1606 (2003) 43–55.
[13] V.M. Ramesh, K. Gibasiewicz, S. Lin, S.E. Bingham, A.N. Webber, Bidirectional electron transfer in photosystem I: accumulation of A0- in a-side or B-side mutants of the axial ligand to chlorophyll A0, Biochemistry 43 (2004) 1369–1375.
[14] S. Santabarbara, I. Kuprov, W.V. Fairclough, S. Purton, P.J. Hore, P. Heathcote, M.C. Evans, Bidirectional electron transfer in photosystem I: determination of two distances between P700+ and A1- in spin-correlated radical pairs, Biochemistry 44 (2005) 2119–2128.
[15] M. Byrdin, S. Santabarbara, F. Gu, W.V. Fairclough, P. Heathcote, K. Redding, F. Rappaport, Assignment of a kinetic component to electron transfer between iron-sulfur clusters F_X and F_A/F_B) of Photosystem I, Biochim. Biophys. Acta 1757 (2006) 1529–1538.
[16] W. Giera, K. Gibasiewicz, V.M. Ramesh, S. Lin, A. Webber, Electron transfer from A to A(1) in Photosystem I from *Chlamydomonas reinhardtii* occurs in both the A and B branch with 25-30-ps lifetime, Phys. Chem. Chem. Phys. 11 (2009) 5186–5191.
[17] T. Berthold, E.D. von Gromoff, S. Santabarbara, P. Stehle, G. Link, O.G. Poluektov, P. Heathcote, C.F. Beck, M.C. Thurnauer, G. Kothe, Exploring the electron transfer pathways in photosystem I by high-time-resolution electron paramagnetic resonance: observation of the B-side radical pair P700(+)A1B(-) in whole cells of the deuterated green alga *Chlamydomonas reinhardtii* at cryogenic temperatures, J. Am. Chem. Soc. 134 (2012) 5563–5576.
[18] R.O. Cohen, G. Shen, J.H. Golbeck, W. Xu, P.R. Chitnis, A.I. Valieva, A. van der Est, Y. Pushkar, D. Stehlik, Evidence for asymmetric electron transfer in cyanobacterial Photosystem I: analysis of a methionine-to-leucine mutation of the ligand to the primary electron acceptor A_0, Biochemistry 43 (2004) 4741–4754.
[19] N. Dashdorj, W. Xu, R.O. Cohen, J.H. Golbeck, S. Savikhin, Asymmetric electron transfer in cyanobacterial Photosystem I: charge separation and secondary electron transfer dynamics of mutations near the primary electron acceptor A_0, Biophys. J. 88 (2005) 1238–1249.
[20] A. Savitsky, O. Gopta, M. Mamedov, J.H. Golbeck, A. Tikhonov, K. Mobius, A. Semenov, Alteration of the axial met ligand to electron acceptor A_0 in Photosystem I: effect on the generation of $P_{700}^{+}A_1^{-}$ radical pairs as studied by W-band transient EPR, Appl. Magn. Reson. 37 (2010) 85–102.
[21] A. van der Est, S. Chirico, I. Karyagina, R. Cohen, G. Shen, J. Golbeck, Alteration of the axial Met ligand to electron acceptor A_0 in Photosystem I: An investigation of electron transfer at different temperatures by multifrequency time-resolved and CW EPR, Appl. Magn. Reson. 37 (2010) 103–121.
[22] S. Santabarbara, I. Kuprov, O. Poluektov, A. Casal, C.A. Russell, S. Purton, M.C. Evans, Directionality of electron-transfer reactions in photosystem I of prokaryotes: universality of the bidirectional electron-transfer model, J. Phys. Chem. B 114 (2010) 15158–15171.
[23] W. Xu, P. Chitnis, A. Valieva, A. van der Est, Y.N. Pushkar, M. Krzystyniak, C. Teutloff, S.G. Zech, R. Bittl, D. Stehlik, B. Zybailov, G. Shen, J.H. Golbeck, Electron transfer in cyanobacterial Photosystem I: I. Physiological and spectroscopic characterization of site-directed mutants in a putative electron transfer pathway from A_0 through A_1 to F_X, J. Biol. Chem. 278 (2003) 27864–27875.
[24] T.W. Johnson, G. Shen, B. Zybailov, D. Kolling, R. Reategui, S. Beauparlant, I.R. Vassiliev, D.A. Bryant, A.D. Jones, J.H. Golbeck, P.R. Chitnis, Recruitment of a foreign quinone into the A_1 site of Photosystem I. I. Genetic and physiological characterization of phylloquinone biosynthetic pathway mutants in *Synechocystis* sp. PCC 6803, J. Biol. Chem. 275 (2000) 8523–8530.
[25] R. Balasubramanian, G. Shen, D.A. Bryant, J.H. Golbeck, Regulatory roles for IscA and SufA in iron homeostasis and redox stress responses in the cyanobacterium *Synechococcus* sp. strain PCC 7002, J. Bacteriol. 188 (2006) 3182–3191.
[26] F.X. Cunningham Jr., Z. Sun, D. Chamovitz, J. Hirschberg, E. Gantt, Molecular structure and enzymatic function of lycopene cyclase from the cyanobacterium *Synechococcus* sp strain PCC7942, Plant Cell 6 (1994) 1107–1121.
[27] H.K. Lichtenthaler, Chlorophylls and carotenoids: pigments of photosynthetic biomembranes, Methods Enzymol. 148 (1987) 350–382.
[28] G. Shen, M.L. Antonkine, A. van der Est, I.R. Vassiliev, K. Brettel, R. Bittl, S.G. Zech, J. Zhao, D. Stehlik, D.A. Bryant, J.H. Golbeck, Assembly of Photosystem I. II. Rubredoxin is required for the *in vivo* assembly of F_X in *Synechococcus* sp. PCC 7002 as shown by optical and EPR spectroscopy, J. Biol. Chem. 277 (2002) 20355–20366.
[29] J. Zhao, R. Li, D.A. Bryant, Measurement of photosystem I activity with photoreduction of recombinant flavodoxin, Anal. Biochem. 264 (1998) 263–270.
[30] E.N. Ushakov, V.A. Nadtochenko, S.P. Gromov, A.I. Vedernikov, N.A. Lobova, M.V. Alfimov, F.E. Gostev, A.N. Petrukhin, O.M. Sarkisov, Ultrafast excited state dynamics of the bi- and termolecular stilbene–viologen charge-transfer complexes assembled via host-guest interactions, Chem. Phys. 298 (2004) 251–261.
[31] T.W. Johnson, B. Zybailov, A.D. Jones, R. Bittl, S. Zech, D. Stehlik, J.H. Golbeck, P. Chitnis, Recruitment of a foreign quinone into the A_1 site of Photosystem I. *In vivo* replacement of plastoquinone-9 by media-supplemented naphthoquinones in phylloquinone biosynthetic pathway mutants of *Synechocystis* sp. PCC 6803, J. Biol. Chem. 276 (2001) 31512–31521.
[32] D. Stehlik, Transient EPR spectroscopy as applied to light-induced functional intermediates along the electron transfer pathway in Photosystem I, in: J. Golbeck (Ed.), Photosystem I: The Light-Driven Plastocyanin:Ferredoxin Oxidoreductase, vol. 24, Springer, Dordrecht, 2006, pp. 361–386.
[33] C.H. Bock, A.J. Vanderest, K. Brettel, D. Stehlik, Nanosecond electron-transfer kinetics in Photosystem-I as obtained from transient EPR at room-temperature, FEBS Lett. 247 (1989) 91–96.
[34] A. van der Est, C. Bock, J. Golbeck, K. Brettel, P. Setif, D. Stehlik, Electron-transfer from the acceptor A1 to the iron-sulfur centers in photosystem-I as studied by transient EPR spectroscopy, Biochemistry US 33 (1994) 11789–11797.
[35] A. Van der Est, A.I. Valieva, Y.E. Kandrashkin, G. Shen, D.A. Bryant, J.H. Golbeck, Removal of PsaF alters forward electron transfer in Photosystem I: Evidence for fast reoxidation of Q_KA in subunit deletion mutants of *Synechococcus* sp. PCC 7002, Biochemistry 43 (2004) 1264–1275.
[36] Y.N. Pushkar, J.H. Golbeck, D. Stehlik, H. Zimmermann, Asymmetric hydrogen-bonding of the quinone cofactor in photosystem I probed by C-13-labeled naphthoquinones, J. Phys. Chem. B 108 (2004) 9439–9448.
[37] Y.N. Pushkar, D. Stehlik, M. van Gastel, W. Lubitz, An EPR/ENDOR study of the asymmetric hydrogen bond between the quinone electron acceptor and the protein backbone in photosystem I, J. Mol. Struct. 700 (2004) 233–241.
[38] R. Agalarov, M. Byrdin, F. Rappaport, G.Z. Shen, D.A. Bryant, A. van der Est, J.H. Golbeck, Removal of the PsaF polypeptide biases electron transfer in favor of the PsaB branch of cofactors in Triton X-100 Photosystem I complexes from *Synechococcus* sp PCC 7002, Photochem. Photobiol. 84 (2008) 1371–1380.
[39] F. Rappaport, B.A. Diner, K. Redding, Optical measurements of secondary electron transfer in Photosystem I, in: J. Golbeck (Ed.), Photosystem I: The Light-Induced Plastocyanin:Ferredoxin Oxidoreductase, vol. 24, Springer, Dordrecht, 2006, pp. 223–244.
[40] J.A. Bautista, F. Rappaport, M. Guergova-Kuras, R.O. Cohen, J.H. Golbeck, J.Y. Wang, D. Beal, B.A. Diner, Biochemical and biophysical characterization of Photosystem I from phytoene desaturase and zeta-carotene desaturase deletion mutants of *Synechocystis* sp. PCC 6803: evidence for PsaA- and PsaB-side electron transport in cyanobacteria, J. Biol. Chem. 280 (2005) 20030–20041.
[41] K. Redding, A. van der Est, The directionality of electron transport in Photosystem I, in: J. Golbeck (Ed.), Photosystem I: The Light-Induced Plastocyanin:Ferredoxin Oxidoreductase, vol. 24, Springer, Dordrecht, 2006, pp. 413–437.
[42] P. Setif, H. Bottin, P. Mathis, Absorption studies of primary reactions in photosystem I. Yield and rate of formation of the P-700 triplet state, Biochim. Biophys. Acta 808 (1985) 112–122.
[43] M.C. Thurnauer, ESR study of the photoexcited triplet state in photosynthetic bacteria, Rev. Chem. Intermed. 3 (1979) 197–230.
[44] P. Setif, K. Brettel, Forward electron transfer from phylloquinone-A_1 to iron sulfur centers in spinach Photosystem I, Biochemistry 32 (1993) 7846–7854.
[45] I. Sieckmann, K. Brettel, C. Bock, A. van der Est, D. Stehlik, Transient electron paramagnetic resonance of the triplet state of P_{700} in Photosystem I: evidence for triplet delocalization at room temperature, Biochemistry 32 (1993) 4842–4847.
[46] K. Brettel, W. Leibl, Electron transfer in Photosystem I, Biochim. Biophys. Acta 1507 (2001) 100–114.
[47] V.V. Ptushenko, D.A. Cherepanov, L.I. Krishtalik, A.Y. Semenov, Semi-continuum electrostatic calculations of redox potentials in Photosystem I, Photosynth. Res. 97 (2008) 55–74.
[48] G.E. Milanovsky, V.V. Ptushenko, J.H. Golbeck, A.Y. Semenov, D.A. Cherepanov, Molecular dynamics study of the primary charge separation reactions in Photosystem I: effect of the replacement of the axial ligands to the electron acceptor A_0, Biochim. Biophys. Acta (2014), http://dx.doi.org/10.1016/j.bbabio.2014.03.001.
[49] B. Zybailov, A. van der Est, S.G. Zech, C. Teutloff, T.W. Johnson, G. Shen, R. Bittl, D. Stehlik, P.R. Chitnis, J.H. Golbeck, Recruitment of a foreign quinone into the A_1 site of Photosystem I. II. Structural and functional characterization of phylloquinone biosynthetic pathway mutants by electron paramagnetic resonance and electron-nuclear double resonance spectroscopy, J. Biol. Chem. 275 (2000) 8531–8539.
[50] A.Y. Semenov, I.R. Vassiliev, A. van der Est, M.D. Mamedov, B. Zybailov, G. Shen, D. Stehlik, B.A. Diner, P.R. Chitnis, J.H. Golbeck, Recruitment of a foreign quinone into the A_1 site of Photosystem I. Altered kinetics of electron transfer in phylloquinone biosynthetic pathway mutants studied by time-resolved optical, EPR, and electrometric techniques, J. Biol. Chem. 275 (2000) 23429–23438.
[51] R.C. Prince, P.L. Dutton, J.M. Bruce, Electrochemistry of ubiquinones, menaquinones and plastoquinones in aprotic solvents, FEBS Lett. 160 (1983) 273–276.
[52] R.C. Prince, P. Lloyd-Williams, J.M. Bruce, P.L. Dutton, Voltammetric measurements of quinones, Methods Enzymol. 125 (1986) 109–119.
[53] C.S. Coates, J. Ziegler, K. Manz, J. Good, B. Kang, S. Milikisiyants, R. Chatterjee, S. Hao, J.H. Golbeck, K.V. Lakshmi, The structure and function of quinones in biological solar energy transduction: a cyclic voltammetry, EPR and hyperfine sub-level correlation (HYSCORE) spectroscopy study of model naphthoquinones, J. Phys. Chem. B 117 (2013) 7210–7220.